Indian Journal of Chemistry
Vol. 62, October 2023, pp. 1061-1080
DOI: 10.56042/ijc.v62i10.6186

Synthesis, characterisation, *in silico* molecular docking and DFT studies of 2,6-bis(4-hydroxy-3-methoxyphenyl)-3,5-dimethylpiperidin-4-one

J Gershom Stuart & J Winfred Jebaraj*

Department of Chemistry, St. John's College, Palayamkottai 627 002, Tamil Nadu, India

(Affiliated to Manonmaniam Sundaranar University, Abishekapatti, Tirunelveli 627 012, Tamil Nadu, India)

E-mail: winfred.chem@stjohnscollege.edu.in

Received 5 January 2023; accepted (revised) 21 September 2023

The target molecule 2,6-bis(4-hydroxy-3-methoxyphenyl)-3,5-dimethylpiperidin-4-one (BHMD) has best binding energy of –7.5 kcal/mol with 5YOK protein of HIV-1 protease. The theoretical studies of the target molecule have been carried out using Gaussian 16W software and viewed by Gaussview 06 software. Bond length, bond angle and dihedral angle of optimized geometry have been performed by DFT method with B3LYP/6-311G (d,p) basis set. The charge transfer and electronic properties of the target molecule have been explained on the basis of highest occupied molecular orbital and lowest unoccupied molecular orbital and its energy values have been used for calculating the global chemical reactivity parameters. In addition to that, molecular electrostatic potential and Mulliken population analysis have been calculated and discussed for predicting the reactive site. NBO analysis has been used to study the charge delocalization and stability of the molecule. NCI and shaded surface map with projection effect of electron localization function have also been studied by Multiwfn 3.8 software.

Keywords: 2,6-Bis(4-hydroxy-3-methoxyphenyl)-3,5-dimethylpiperidin-4-one, DFT, NBO, NCI, FT-IR

Over the past decades, the HIV-1 epidemic is still believed as a global public health problem, but great advances have been made in fighting it by antiretroviral therapy (ART)[1]. Antiretroviral therapy has made a consequential progress in the treatment for human immunodeficiency virus type-1 (HIV-1)[2]. By means of nucleoside and non-nucleoside reverse transcriptase and protease inhibitors, the antiretroviral therapy is done for human immunodeficiency virus type-1 (HIV-1) infection which has adduced to become favourable for patients because of the routine dosing regimen and minimized intake of orally ingestible pills[3,4].

Piperidones (also known as piperidinones) is a family of saturated heterocyclic organic compounds which are used as an intermediate in the manufacture of chemicals and are found to possess diversified pharmacological activity and form an essential part of the molecular structure of some drugs[5,6]. Piperidone based compounds have received much attention for drug discovery research. The piperidone structure may be a flexible moiety due to the inclusion of a carbonyl group and a secondary amine group, both of which include alpha-protons, and finds extensive uses in synthetic organic chemistry, pharmaceutical chemistry and different sections of chemistry[7]. In addition to the fascinating structural features, these are also of pharmaceutical significance as they exhibit a broad variety of biological activities such as antioxidant[8], antimicrobial[9], anticancer[10], apoptosis[11], antibacterial, antitubercular[12], antipyretic[13,14], anti-inflammatory[15,16], antitumour agents[17], antimalarial[18,19], antiplasmodial[20] and antihypertensive agents[21].

A trend toward using *in silico* chemistry and molecular modelling for computer-aided drug creation has recently gained traction. The main benefit of the *in silico* drug design was cost effective in research and development of drugs[22]. The protein-ligand interaction plays a significant role in structural based drug designing[23]. In like manner, the selected piperidin-4-one derivative may carry immense potential in HIV treatment and identified as the most potential new compound with active nature against 5YOK with a binding affinity value of –7.5 kcal/mol for that reason the present investigation was performed to monitor the piperidin-4-one derivative for antiretroviral activity.

Materials and methods

Docking process

The protein data bank (http://www.rcsb.org.pdb) provided the crystal structure of *HIV-1 Protease* in

complex with inhibitor KNI-1657 (PDB ID: 5YOK) employed in the work[24]. The 5YOK was discovered using the X-ray diffraction technique, which yielded a resolution of 0.85 Å. The Discovery Studio 4.0 Visualizer tool was used to remove all solvent molecules as well as bounded compounds (ligands and cofactors) from the receptor before saving it in PDB format[25]. ASPIN CO (http://www.apin.co.uk/?op=groups&group=Aromatic+Aldehydes+%26+Derivatives+(substituted) and Open Molecule website (http://www.openmolecules.org/name2structure.html) provided the names of several aromatic aldehydes. Chemsketch software[26] was used to design the 2D structures of 673 piperidone derivatives based on the structures. Numerous elements and functional groups such as Cl, Br, I, NH_2, OH, OMe, NO_2, *etc*., were substituted in various positions as mono, di, or tri substitutions. Finally, the most effective docking model was chosen for further research. The standard preparation procedure for piperidone was illustrated in Scheme 1 [27]. The Avogadro tool was used to minimise all the piperidone derivatives[28]. The PDB format was used to preserve the minimised structures. PyRx software[29] and the AutoDockprogramme[30] were used to dock a series of 673 piperidin-4-one ligands with prepared protein 5YOK. PyMOL[31] was used to view and evaluate the docking results.

Computational details

All the theoretical calculations were described within the framework of density functional theory (DFT) methodology as implemented in Gaussian 16W package[32]. The widely used density function Becke3-Lee-Yang-Parr (B3LYP) level[33] with triple zeta basis set in conjunction with diffuse and polarize function 6-311G (d,p) basis set was employed in the program for the calculations. Gaussview 06 was a molecular visualisation programme for observing the characteristics of molecules[34]. The structural characteristics such as bond length, bond angle and dihedral angle have been computed theoretically. DFT with the B3LYP/6-311G (d,p) technique was used to determine the target molecule's molecular electrostatic potential, Mulliken population analysis, and natural bond orbital analysis. HOMO and LUMO values were used to calculate ionization potential, electron affinity, global softness, electronegativity, chemical hardness, electrophilicity index, nucleophilicity index and several quantum chemical parameters. The bond topology analysis, electron localization function (ELF)[35], localized orbital locator (LOL) and non-covalent interactions were studied and reduced density gradients[36] were analysed by Multiwfn 3.8 [37].

Experimental Section

The compound (BHMD) was prepared by adopting the procedure invented by Noller and Baliah with a few minor modifications. To a solution of ammonium acetate (0.05 mol) in absolute ethanol (60 mL), 4-Hydroxy-3-methoxybenzaldehyde (vanillin) (0.1 mol) and Diethyl ketone (0.05 mol) were added and the contents were refluxed for in a 250 mL RB flask equipped with a water condenser 30 minutes. Further the contents were set aside at room temperature overnight. The separated crude sample was thoroughly cleaned with absolute alcohol before being refined by recrystallization from ethanol (Scheme 1). The obtained solution was filtered by Whatman 41 filter paper and the filtered solution was preserved in a dust free environment and it was carefully taken to minimize the temperature gradient and mechanical shock. The free bases were converted to the hydrochlorides by the addition of concentrated hydrochloric acid into an ether solution of the base. When an oil separated, the base was converted directly to the hydrochloride and purified by crystallization. The hydrochloride was converted to the free base by adding aqueous ammonia to an alcohol solution, and the base precipitated by dilution

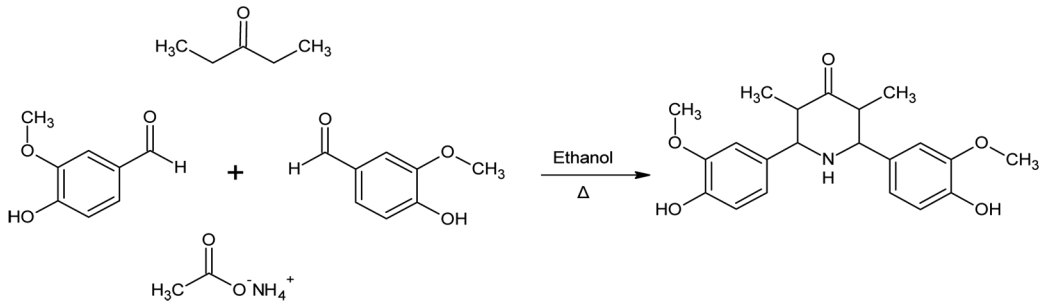

Scheme 1 — Ligand designing route

with water. After 7 to 10 days, a significant amount of high-quality yield was extracted from the solution.

The FT-IR spectroscopy of BHMD was recorded in the frequency range of 400–4000 cm^{-1} using KBr pellet on SHIMADZU model instrument.

Result and Discussion

Molecular docking studies

In this docking study by using PyRx software, a freshly developed series of 673 ligands were docked with the 5YOK protein of HIV-1 Protease. The ligand, 2,6-bis(4-hydroxy-3-methoxyphenyl)-3,5-dimethylpiperidin-4-one was identified as the most potential new compound with active nature against 5YOK with a binding affinity value of -7.5 kcal/mol which was compared with some of the approved HIV-1 drugs which were also docked against 5YOK protein and their binding values were tabulated in Table 1. It was found that the target molecule was having the best docking score which was equal to atazanavir which has best docking score.

The non-toxic and organically dynamic character of the title compound was directed by feedback on drug likeness limitations. The evaluation of drug similarity was necessary to rule out substances that were not suitable for use as a dynamic medication. Lipinski's rule of five was a simple criterion for determining whether a chemical molecule was physiologically dynamic or not[38]. The Table 2 lists the drug similarity requirements for the title compound including molar refractivity, AlogP, the number of hydrogen bond donors and acceptors (HBD and HBA) and the number of rotatable bonds. According to Lipinski's rule of five[39], the limits of drug similarity were predictable, resulting in standards within the superior range. The number of HBD and HBA were 3 and 6, respectively, while the number of rotatable bonds was 4. At this point, all of the numbers were considered to be within the range. The value of log P was observed to be 3.341898, indicating that the molecule is hydrophobic/lipophilic. The molar refractivity values was 101.270264 which was considered to be within the appropriate limits. The nontoxic and biologically active character of the title compounds was revealed by the investigation of drug likeness parameters. Furthermore, docking simulations were used to investigate the relation of the title compounds as a ligand with the target protein. It has a good drug-likeness value and it was found to be 0.23 by Molsoft prediction (http://www.molsoft.com/) and given in Table 2.

Table 1 — Binding value of drugs

S.No	Drug name	Binding value (kcal/mol)
1	2,6-Bis(4-hydroxy-3-methoxyphenyl)-3,5-dimethylpiperidin-4-one	–7.5
2	Atazanavir	–7.5
3	Zidovudine	–7.3
4	Ritonavir	–7.1
5	Efavirenz	–7.0
6	Nevirapine	–7.0
7	Fosamprenavir	–6.9
8	Abacavir	–6.8
9	Cobicistat	–6.8
10	Tenofovirdisoproxil fumarate	–6.4

Molecular geometry

Optimized parameter of the target molecule

2,6-bis(4-hydroxy-3-methoxyphenyl)-3,5-dimethylpiperidin-4-one was a chemical compound with molecular formula $C_{21}H_{25}NO_5$.The 2D and 3D representations for the target molecule were given in Fig. 1. The atom numbering scheme for the title compound was shown in Table 3. It has 21 carbon atoms, 25 hydrogen atoms, 5 oxygen atoms and a nitrogen atom with a total of 52 atoms. It has 198 electrons. It was a neutral and singlet system. The carbons 1, 2, 3, 5, 6 were present in piperidone ring. The other carbons were present in the six membered aromatic rings and in side chains.

Bond length

The bond length was defined to be the average distance between the nuclei of two bonded atoms bonded together in any given molecule and in this calculated by DFT/ B3LYP method using 6-311G(d,p) basis set for BHDM. In the present investigation, the bond angle for C-C in the piperidone was around 1.5 Å due to the presence of the electronegative substitutes of C3-O19 and N4-H30 in piperidone ring, while the C-N bond lengths were 1.4782 and 1.4758 Å for C2-N4 and C6-N4 bond respectively. In the substituted piperidone, the phenyl ring carbon atoms exert a large attraction on

Table 2 — Drug likeness parameters of title compound

Descriptors	Value	Expected range
Hydrogen bond donor (HBD)	3	<5
Hydrogen bond acceptors (HBA)	6	<10
AlogP	3.341898	<5
Molecular weight (dalton)	371.000000	<500
Number of rotatable bonds	4	<10
Molar refractivity	101.270264	40-130

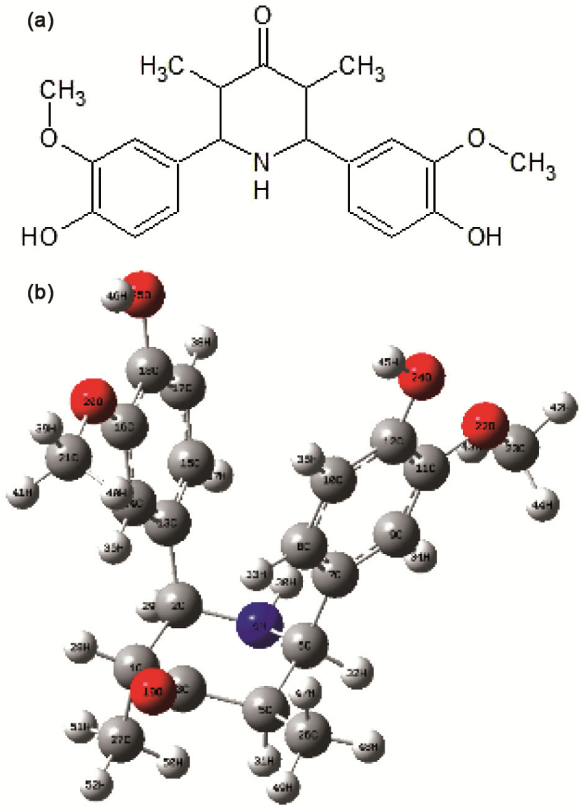

Fig. 1 — (a) 2D and (b) optimized 3D structure of BHMD with atom numbering schemes

the valence electron cloud of the H atom resulting in a decrease in the C-C bond lengths around 1.39 Å. The C-H bond lengths were calculated as around 1.08 Å for phenyl rings and piperidone rings and around 1.09 Å for isopentyl group that were typical C-H single bond lengths. The longest bond length was at C5-C6 with a distance of 1.5595 Å and the shortest bond length was found in O24-H45 with a distance of 0.9626 Å confirms the stability of the title molecule as the bond length decreases and bond energy increases, which gives greater stability to the molecule[40]. In aromatic compounds, if the ring carbon atoms were bonded to H atom with σ bond may lead to change (decrease) in the bond length and also reduce the electron density at the ring carbon atom[41]. The optimized geometrical parameters of BHDM were listed in Table 4.

Table 3 — Atom list of the optimized target molecule

1	C	**9**	C	**17**	C	**25**	O	**33**	H	**41**	H	**49**	H
2	C	**10**	C	**18**	C	**26**	C	**34**	H	**42**	H	**50**	H
3	C	**11**	C	**19**	O	**27**	C	**35**	H	**43**	H	**51**	H
4	N	**12**	C	**20**	O	**28**	H	**36**	H	**44**	H	**52**	H
5	C	**13**	C	**21**	C	**29**	H	**37**	H	**45**	H	–	–
6	C	**14**	C	**22**	O	**30**	H	**38**	H	**46**	H	–	–
7	C	**15**	C	**23**	C	**31**	H	**39**	H	**47**	H	–	–
8	C	**16**	C	**24**	O	**32**	H	**40**	H	**48**	H	–	–

Table 4 — Bond length of the optimized geometrical parameters of BHMD at B3LYP/6-311G (d,p) level of theory

Code No	Atoms set	Distance (Å)	Code No	Atoms set	Distance (Å)
R1	(C1,C2)	1.550	R28	(C13,C14)	1.403
R2	(C1,C3)	1.527	R29	(C13,C15)	1.396
R3	(C1,C27)	1.542	R30	(C14,C16)	1.390
R4	(C1,H28)	1.091	R31	(C14,H36)	1.081
R5	(C2,N4)	1.476	R32	(C15,C17)	1.393
R6	(C2,C13)	1.539	R33	(C15,H37)	1.086
R7	(C2,H29)	1.097	R34	(C16,C18)	1.405
R8	(C3,C5)	1.523	R35	(C16,O20)	1.375
R9	(C3,O19)	1.215	R36	(C17,C18)	1.388
R10	(N4,C6)	1.478	R37	(C17,H38)	1.083
R11	(N4,H30)	1.013	R38	(C18,O25)	1.362
R12	(C5,C6)	1.560	R39	(O20,C21)	1.423
R13	(C5,C26)	1.527	R40	(C21,H39)	1.089
R14	(C5,H31)	1.097	R41	(C21,H40)	1.095
R15	(C6,C7)	1.531	R42	(C21,H41)	1.095
R16	(C6,H32)	1.096	R43	(O22,C23)	1.418
R17	(C7,C8)	1.390	R44	(C23,H42)	1.089
R18	(C7,C9)	1.406	R45	(C23,H43)	1.097
R19	(C8,C10)	1.396	R46	(C23,H44)	1.096
R20	(C8,H33)	1.081	R47	(O24,H45)	0.963
R21	(C9,C11)	1.391	R48	(O25,H46)	0.967
R22	(C9,H34)	1.084	R49	(C26,H47)	1.089
R23	(C10,C12)	1.388	R50	(C26,H48)	1.094
R24	(C10,H35)	1.087	R51	(C26,H49)	1.092
R25	(C11,C12)	1.410	R52	(C27,H50)	1.091
R26	(C11,O22)	1.362	R53	(C27,H51)	1.093
R27	(C12,024)	1.364	R54	(C27,H52)	1.093

Bond angle

A bond angle is the angle formed between three atoms across at least two bonds. In this work, the obtained results show that the C-N-H bond angles in the piperidone ring were found to be 110.372° and 109.7931° for C2-N4-H30 and C6-N4-H30 respectively, which was similar as expected. The deviation from perfect tetrahedral angle of 109.5° was due to the presence of a lone pair electrons in N atom. The largest bond angle was observed in C14-C16-C20 with the angle of 125.6314° and the shortest bond angle was observed in C6-C5-H31 with the angle of 103.3928°.The selected geometrical parameters for compound were listed in Table 5.

Dihedral angle

The angle formed by two intersecting planes or half-planes was known as a dihedral angle. It is the

Table 5 — Bond angle of the optimized geometrical parameters of BHMD at B3LYP/6-311G (d,p) level of theory

Code No	Atoms set	Bond angle (°)	Code No	Atoms set	Bond angle (°)
A1	(C2,C1,C3)	109.8	A48	(C11,C12,O24)	117.3
A2	(C2,C1,C27)	111.0	A49	(C2,C13,C14)	123.3
A3	(C2,C1,H28)	109.8	A50	(C2,C13,C15)	118.5
A4	(C3,C1,C27)	111.4	A51	(C14,C13,C15)	118.0
A5	(C3,C1,H28)	106.6	A52	(C13,C14,C16)	120.5
A6	(C27,C1,H28)	107.9	A53	(C13,C14,H36)	120.4
A7	(C1,C2,N4)	107.9	A54	(C16,C14,H36)	118.9
A8	(C1,C2,C13)	114.5	A55	(C13,C15,C17)	121.5
A9	(C1,C2,H29)	106.3	A56	(C13,C15,H37)	119.8
A10	(C4,C2,C13)	116.9	A57	(C17,C15,H37)	118.5
A11	(N4,C2,H29)	104.3	A58	(C14,C16,C18)	120.6
A12	(C13,C2,H29)	105.5	A59	(C14,C16,C20)	125.6
A13	(C1,C3,C5)	115.1	A60	(C18,C16,C20)	113.7
A14	(C1,C3,O19)	121.8	A61	(C15,C17,C18)	120.0
A15	(C5,C3,O19)	123.0	A62	(C15,C17,H38)	121.3
A16	(C2,N4,C6)	119.8	A63	(C18,C17,H38)	118.5
A17	(C2,N4,H30)	110.3	A64	(C16,C18,C17)	119.0
A18	(C6,N4,H30)	109.7	A65	(C16,C18,O25)	120.4
A19	(C3,C5,C6)	110.9	A66	(C17,C18,O25)	120.5
A20	(C3,C5,C26)	113.7	A67	(C16,O20,C21)	118.4
A21	(C3,C5,H31)	104.3	A68	(O20,C21,H39)	105.9
A22	(C6,C5,C26)	115.1	A69	(O20,C21,H40)	111.4
A23	(C6,C5,H31)	103.3	A70	(O20,C21,H41)	111.1
A24	(C26,C5,H31)	108.2	A71	(H39,H21,H40)	109.4
A25	(N4,C6,C5)	108.0	A72	(H39,C21,H41)	109.4
A26	(N4,C6,C7)	116.1	A73	(H40,C21,H41)	109.2
A27	(N4,C6,H32)	104.2	A74	(C11,O22,C23)	118.2
A28	(C5,C6,C7)	116.6	A75	(O22,C23,H42)	105.7
A29	(C5,C6,H32)	105.1	A76	(O22,C23,H43)	111.6
A30	(C7,C6,H32)	105.2	A77	(O22,C23,H44)	111.6
A31	(C6,C7,C8)	124.9	A78	(H42,C23,H43)	109.2
A32	(C6,C7,C9)	116.9	A79	(H42,C23,H44)	109.2
A33	(C8,C7,C9)	118.0	A80	(H43,C23,H44)	109.2
A34	(C7,C8,C10)	120.4	A81	(C12,O24,H45)	108.4
A35	(C7,C8,H33)	120.9	A82	(C18,O25,H46)	106.9
A36	(C10,C8,H33)	118.6	A83	(C5,C26,H47)	112.2
A37	(C7,C9,C11)	122.0	A84	(C5,C26,H48)	110.2
A38	(C7,C9,H34)	118.6	A85	(C5,C26,H49)	110.1
A39	(C11,C9,H34)	119.2	A86	(H47,C26,H48)	108.1
A40	(C8,C10,C12)	121.3	A87	(H47,C26,H49)	107.6
A41	(C8,C10,H35)	119.7	A88	(H48,C26,H49)	108.3
A42	(C12,C10,H35)	118.9	A89	(C1,C27,H50)	111.1
A43	(C9,C11,C12)	118.9	A90	(C1,C27,H51)	109.5
A44	(C9,C11,O22)	125.3	A91	(C1,C27,H52)	111.3
A45	(C12,C11,O22)	115.6	A92	(H50,C27,H51)	107.9
A46	(C10,C12,C11)	119.1	A93	(H50,C27,H52)	109.1
A47	(C10,C12,O24)	123.5	A94	(H51,C27,H52)	107.6

clockwise angle between half-planes that passes across two sets of three atoms which have two atoms in common. Dihedral angles were used to identify the molecular conformation[42]. Stereochemical arrangements corresponding to angles can be defined by the two types of terms can be combined so as to define four ranges of angle such as

(i) 0° to ±30° synperiplanar(sp)
(ii) 30° to 90° and −30° to −90° synclinal (sc)
(iii) 90° to 150° and −90° to −150° anticlinal (ac)
(iv) ±150° to 180° antiperiplanar (ap).

The synperiplanar conformation was also known as the syn-conformation or cis-conformation. The antiperiplanar as anti-conformation or trans-conformation and synclinal as gauche or skew.

From the Table 6, it was clear that synperiplanar(sp), antiperiplanar(ap), anticlinal (ac) and synclinal (sc) were present in the target molecule.

Table 6 — Dihedral angle of the optimized geometrical parameters of BHMD at B3LYP/6-311G (d,p) level of theory

Code no	Atoms	Dihedral angle (°)	Conformation	Code no	Atoms	Dihedral angle (°)	Conformation
1	C3-C1-C2-N4	51.8	+SC	68	N4-C6-C7-C9	–85.1	–SC
2	C3-C1-C2-C13	–80.3	–AC	69	C5-C6-C7-C8	–35.9	–SC
3	C3-C1-C2-H29	163.3	+AP	70	C5-C6-C7-C9	145.5	+AC
4	C27-C1-C2-N4	–71.8	–SC	71	H32-C6-C7-C8	–152.0	–AP
5	C27-C1-C2-C13	155.8	+AP	72	H32-C6-C7-C9	29.4	+SP
6	C27-C1-C2-H29	39.6	+SC	73	C6-C7-C8-C10	–177.4	–AP
7	H28-C1-C2-N4	168.8	+AP	74	C6-C7-C8-H33	2.5	+SP
8	H28-C1-C2-C13	36.5	+SC	75	C9-C7-C8-C10	1.0	+SP
9	H28-C1-C2-H29	–79.6	–SC	76	C9-C7-C8-H33	–179.0	–AP
10	C2-C1-C3-C5	–54.1	–SC	77	C6-C7-C9-C11	177.3	+AP
11	C2-C1-C3-C19	126.2	+AC	78	C6-C7-C9-H34	–2.9	–SP
12	C27-C1-C3-C5	69.3	+SC	79	C8-C7-C9-C11	–1.1	–SP
13	C27-C1-C3-C19	–110.2	–AC	80	C8-C7-C9-H34	178.4	+AP
14	H28-C1-C3-C5	–173.1	–AP	81	C7-C8-C10-C12	–0.1	–SP
15	H28-C1-C3-O19	7.25	+SP	82	C7-C8-C10-H35	179.7	+AP
16	C2-C1-C27-H50	48.9	+SC	83	H33-C8-C10-C12	179.9	+AP
17	C2-C1-C27-H51	–70.2	–SC	84	H33-C8-C10-H35	–0.2	–SP
18	C2-C1-C27-H52	170.8	+AP	85	C7-C9-C11-C12	0.4	+SP
19	C3-C1-C27-H50	–73.8	–SC	86	C7-C9-C11-O22	179.9	+AP
20	C3-C1-C27-H51	166.9	+AP	87	H34-C9-C11-C12	–179.2	–AP
21	C3-C1-C27-H52	48.0	+SC	88	H34-C9-C11-O22	0.3	+SP
22	H28-C1-C27-H50	169.3	+AP	89	C8-C10-C12-C11	–0.6	–SP
23	H28-C1-C27-H51	50.1	+SC	90	C8-C10-C12-O24	179.9	+AP
24	H28-C1-C27-H52	–68.7	–SC	91	H35-C10-C12-C11	179.4	+AP
25	C1-C2-N4-C6	–57.6	–SC	92	H35-C10-C12-O24	0.0	+SP
26	C1-C2-N4-H30	173.3	+AP	93	C9-C11-C12-C10	0.4	+SP
27	C13-C2-N4-C6	73.3	+SC	94	C9-C11-C12-O24	179.9	+AP
28	C13-C2-N4-H30	–55.7	–SC	95	O22-C11-C12-C10	–179.0	–AP
29	H29-C2-N4-C6	–170.4	–AP	96	O22-C11-C12-O24	0.3	+SP
30	H29-C2-N4-H30	60.4	+SC	97	C9-C11-O22-H23	0.3	+SP
31	C1-C2-C13-C14	5.7	+SP	98	C12-C11-O22-H23	179.8	+AP
32	C1-C2-C13-C15	–171.8	–AP	99	C10-C12-O24-H45	–1.9	–SP
33	N4-C2-C13-C14	–122.0	–AC	100	C11-C12-O24-H45	178.6	+AP
34	N4-C2-C13-C15	60.3	+SC	101	C2-C13-C14-C16	–178.5	–AP
35	H29-C2-C13-C14	122.4	+AC	102	C2-C13-C14-H36	3.0	+SP
36	H29-C2-C13-C15	–55.1	–SC	103	C15-C13-C14-C16	–0.9	–SP
37	C1-C3-C5-C6	52.5	+SC	104	C15-C13-C14-H36	–179.3	–AP
38	C1-C3-C5-C26	–175.7	–AP	105	C2-C13-C15-C17	178.7	+AP
39	C1-C3-C5-H31	–58.1	–SC	106	CC2-C13-C15-H37	–0.9	–SP
40	O19-C3-C5-C6	–127.7	–AC	107	C14-C13-C15-C17	1.0	+SP
41	O19-C3-C5-C26	3.8	+SP	108	C14-C13-C15-H37	–178.6	–AP
42	O19-C3-C5-H31	121.5	+AC	109	C13-C14-C16-C18	0.3	+SP
43	C2-N4-C6-C5	55.5	+SC	110	C13-C14-C16-C20	–179.3	–AP
44	C2-N4-C6-C7	–77.7	–SC	111	H36-C14-C16-C18	178.7	+AP
45	C2-N4-C6-H32	167.0	+AP	112	H36-C14-C16-C20	–0.8	–SP

(*Contd.*)

Table 6 — Dihedral angle of the optimized geometrical parameters of BHMD at B3LYP/6-311G (d,p) level of theory (*Contd*.)

Code no	Atoms	Dihedral angle (°)	Conformation	Code no	Atoms	Dihedral angle (°)	Conformation
46	H30-N4-C6-C5	–175.0	–AP	113	C13-C15-C17-C18	–0.4	–SP
47	H30-N4-C6-C7	51.5	+SC	114	C13-C15-C17-H38	179.9	+AP
48	H30-N4-C6-H32	–63.6	–SC	115	H37-C15-C17-C18	179.2	+AP
49	C3-C5-C6-N4	–48.5	–SC	116	H37-C15-C17-H38	–0.3	–SP
50	C3-C5-C6-C7	84.4	+SC	117	C14-C16-C18-C17	0.2	+SP
51	C3-C5-C6-H32	–159.4	–AP	118	C14-C16-C18-C25	179.9	+AP
52	C26-C5-C6-N4	–179.4	–AP	119	C20-C16-C18-C17	179.9	+AP
53	C26-C5-C6-C7	–46.4	–SC	120	C20-C16-C18-O25	–0.4	–SP
54	C26-C5-C6-H32	69.6	+SC	121	C14-C16-O20-C21	–4.2	–SP
55	H31-C5-C6-N4	62.7	+SC	122	C18-C16-O20-C21	176.0	+AP
56	H31-C5-C6-C7	–164.2	–AP	123	C15-C17-C18-C16	–0.1	–SP
57	H31-C5-C6-H32	–48.1	–SC	124	C15-C17-C18-O25	–179.8	–AP
58	C3-C5-C26-H47	–60.6	–SC	125	H38-C17-C18-C16	179.3	+AP
59	C3-C5-C26-H48	178.7	+AP	126	H38-C17-C18-O25	–0.3	–SP
60	C3-C5-C26-H49	59.2	+SC	127	C16-C18-O25-H46	–0.8	–SP
61	C6-C5-C26-H47	68.8	+SC	128	C17-C18-O25-H46	178.8	+AP
62	C6-C5-C26-H48	–51.7	–SC	129	C16-O20-C21-H39	–178.7	–AP
63	C6-C5-C26-H49	–171.2	–AP	130	C16-O20-C21-H40	62.2	+SC
64	H31-C5-C26-H47	–176.0	–AP	131	C16-O20-C21-H41	–59.9	–SC
65	H31-C5-C26-H48	63.3	+SC	132	C11-O22-C23-H42	179.7	+AP
66	H31-C5-C26-H49	–56.1	–SC	133	C11-O22-C23-H43	61.0	+SC
67	N4-C6-C7-C8	93.2	+AC	134	C11-O22-C23-H44	–61.5	–SC

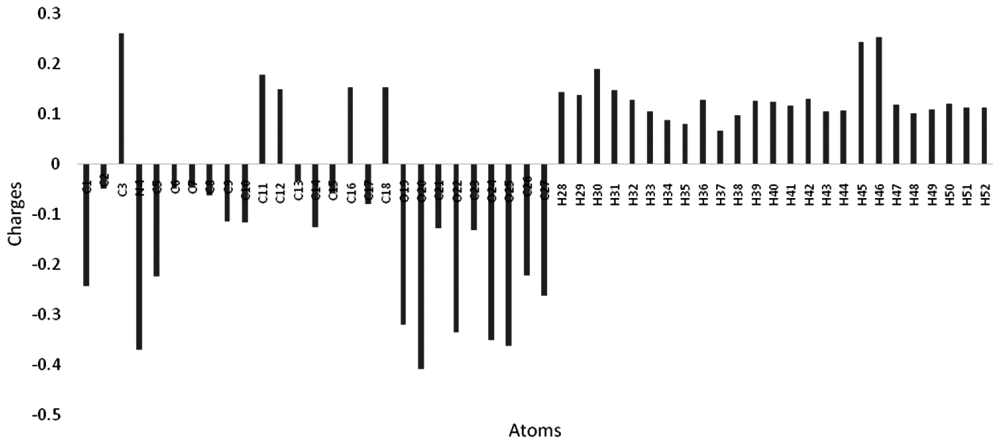

Fig. 2 — The Mulliken atomic charge distribution of target molecule

Mulliken atomic charges

Mulliken atomic charge analysis of the title molecule was carried out using the B3LYP method with 6-311G (d,p) basis set and the results were presented in Fig. 2. In the title molecule, both positive and negative charges were found over different atoms. All the hydrogen atoms were positively charged and the atoms H45 (0.2447 a.u.) and H46 (0.2532a.u.) possess higher values than other atoms as expected, due to their involvement in intramolecular hydrogen bonding interactions. The nitrogen atom in the piperidone ring was found to possess great negative charge (-0.3708 a.u.). All carbon atoms were negatively charged except C3, C11, C12, C16 and C18 which were attached to O19, O22, O24, O28 and O25 atoms respectively which were most electronegative atoms and was clear cut evidence for deprotonation[43]. The results in the Table 7 reveals that C3 has the highest positive value of 0.2609 a.u. and the least electronegative atom was O20 with a value of -0.4091a.u. of the compound.

Molecular electrostatic potential analysis

The molecular electrostatic potential MEP was an important descriptor for the better understanding of nucleophilic reactive sites and electrophilic reactive sites as well as hydrogen bonding interactions considering the electronic charge density distribution

Table 7 — Mulliken charge of BHMD molecule

Atom no	Mulliken charge (a.u.)	Atom no	Mulliken charge (a.u.)
C1	–0.2440	C27	–0.2624
C2	–0.0485	H28	0.1440
C3	0.2609	H29	0.1380
N4	–0.3708	H30	0.1907
C5	–0.2236	H31	0.1469
C6	–0.0490	H32	0.1276
C7	–0.0467	H33	0.1062
C8	–0.0626	H34	0.0886
C9	–0.1135	H35	0.0811
C10	–0.1160	H36	0.1289
C11	0.1775	H37	0.0665
C12	0.1493	H38	0.0978
C13	–0.0333	H39	0.1260
C14	–0.1256	H40	0.1252
C15	–0.0580	H41	0.1168
C16	0.1542	H42	0.1308
C17	–0.0803	H43	0.1054
C18	0.1528	H44	0.1078
O19	–0.3195	H45	0.2447
O20	–0.4091	H46	0.2532
C21	–0.1278	H47	0.1181
O22	–0.3367	H48	0.1007
C23	–0.1323	H49	0.1096
O24	–0.3506	H50	0.1203
O25	–0.3626	H51	0.1126
C26	–0.2228	H52	0.1131

around oxygen- nitrogen- chlorine and neighboring hydrogen and carbon atoms[44-47]. Also the 3D visualization of MEP insights for molecular interaction and charge distribution within the molecule. MEP was carried out at B3LYP/6-311G (d,p) level optimized geometry using Gauss view 6.0 software program and the MEP map was shown in Fig. 3. The molecular electrostatic potential MEP was given in a colour code which increases in the order red < green < blue indicating negative, neutral and positive potentials respectively[48]. The electrostatic potential of the target molecule ranges from –6.017 e^{-2} to +6.017 e^{-2}. The different electrostatic potentials at the surfaces were characterized by distinguished colours *i.e.*, red colour indicates the most negative regions of electrostatic potential; blue colour reflects the most positive regions of electrostatic potential and of green implies near zero potential regions. The red colour spread over the oxygen atoms O19, O22 and O25 corresponds to the negative region of electrostatic potential. Also N4and hydrogen atoms were surrounded by blue colour means the positive region of potential. These were the evident of reactive sites of electrophilic and nucleophilic attacks of the compound. The more dominant green colour over the MEP surface indicates

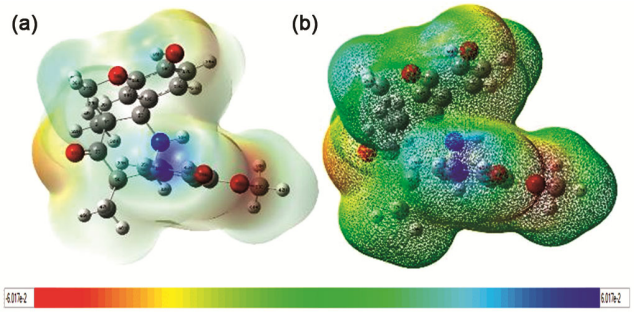

Fig. 3 — The electrostatic potential surface of BHMD (a) transparent and (b) Mesh format

that the electrostatic potential was midway between the vicinity of red and blue region. The residuals species were surrounded by zero potential.

Global reactivity

The Highest Occupied Molecular Orbital (HOMO) and Lowest Unoccupied Molecular Orbital (LUMO) were the principal or bitals participating in the chemical reactivity, kinetic stability, chemical hardness and optical polarizability[49-53]. The absorbance and emission of a fluorescent compound were directly related to the energy of these electronic transitions. To provide a reasonable qualitative indication of the excitation properties- HOMO and LUMO for the target compound were investigated. HOMO was the highest molecular orbital which represents the capability to donate an electron. The lowest molecular orbital LUMO represents the capability of accepting an electron[54,55]. The HOMO and LUMO energies and HOMO–LUMO band gap were predicted from the B3LYP method to investigate the solvent effects on these energies and band gaps (Table 8). The HOMO-LUMO energy values of the title molecule were calculated as -5.5174 eV and -0.9339 eV respectively and the energy gap ΔE was found to be 4.5835 eV. The low energy gap between HOMO and LUMO levels facilitates charge transfer interactions as well as possible proton transfer was the formation of molecule.

HOMO-LUMO energy values were the basis for calculating the global chemical reactivity parameters such as Ionization potential (*I*),electron affinity (*A*), chemical hardness (η), global softness (*s*), electro negativity (χ), chemical potential (μ) electrophilicity index (ω), electron accepting (ω^{+}) and donating capability (ω^{-}), chemical softness (σ), optical softness (σ_0), nucleophilicity index (N) and additional electronic charges (ΔN_{max}) were calculated[56] as these

Table 8 — Calculated quantum chemical parameters of target molecule

S. No	Quantum chemical parameters	eV
1	E_{LUMO}	–0.9339
2	E_{HOMO}	–5.5174
3	Energy band gap E_{HOMO} -E_{LUMO}	4.5835
4	Ionization potential I = -E_{HOMO}	5.5174
5	Electron affinity A = -E_{LUMO}	0.9339
6	Chemical hardness η= I-A/2	2.2917
7	Global softness s = 1/2η	0.2181
8	Electronegativity χ = I+A/2	3.2256
9	Chemical potential μ= -I+A/2	–3.2256
10	Electrophilicity index ω= $\frac{\mu 2}{2\eta}$	2.2699
11	Electron accepting $\omega^{+} = \frac{I+3A2}{16I-A}$	0.9437
12	Donating capability $\omega^{-} = \frac{3I+A2}{16I-A}$	4.1697
13	Chemical softness $\sigma = \frac{1}{\eta}$	0.4363
14	Optical softness $\sigma_0 = \frac{1}{\Delta E}$	0.2181
15	Nucleophilicity index $N = \frac{1}{\omega}$	0.4405
16	Additional electronic charges $\Delta N_{max} = \frac{-\mu}{\eta}$	1.4075

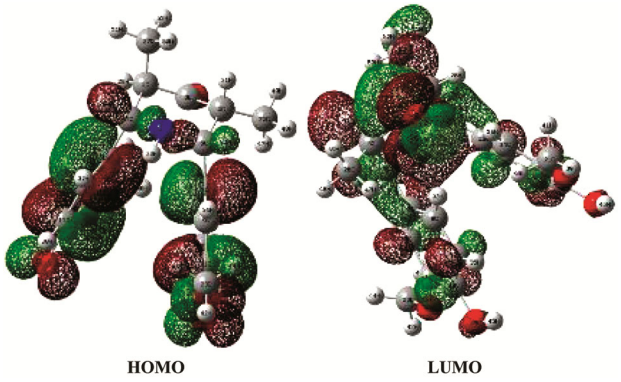

Fig. 4 — Frontier molecular orbital plot for BHMD

parameters were playing a vital role in determining the chemical stability and biological activity of the system and were presented in Table 8. The HOMOs and LUMOs in Fig. 4(a) and Fig. 4(b) (HOMO-LUMO cloud distributions) were obtained and simulated from the optimized molecular geometry using .chkfile at B3LYP/6-311G (d,p) functional levels of the title compund.

Natural bonding orbital (NBO) analysis

NBO analysis was used to find the possible interactions involving the bond orbitals, electron delocalization, bond bending effect, intra- and intermolecular charge transfer (ICT) and identification of hydrogen bonding[57,58]. Larger the E(2) (energy of hyper conjugative interactions) value, the more intensive was the interaction between electron donors and electron acceptors, *i.e.*, the more donating tendency from electron donors to electron acceptors the greater the extent of conjugation of the whole system. Delocalization of electron density between occupied Lewis-type (bond or lone pair) NBO orbitals and formally unoccupied (anti-bond or Rydberg) non-Lewis NBO orbitals correspond to a stabilizing donor–acceptor interactions. The natural bond orbital (NBO) analysis of the target molecule was performed by the method of B3LYP/6-311G (d,p) level in order to elucidate the intra-molecular, re-hybridization and delocalization of electron density within the molecule. The delocalization of electron π* (C14 - C16) to π*(C13 - C15) interaction with enormous stabilization energy of about 244.81 kcal/mol which leads to intermolecular charge transfer process enhancing optical properties of the target molecule. In this molecule, the intramolecular interactions were formed by the orbital overlaps through π- π* interactions such as π(C7 – C8) to π*(C9 – C11), π (C7 - C8) to π*(C10 - C12), π(C13 - C15) to π*(C14 - C16), π(C13 - C15) to π*(C17 - C18), π(C14 - C16) to π*(C13 - C15), π(C14 - C16) to π*(C17 - C18), π(C17 - C18) to π*(C13 - C15) and π(C17 - C18) to π*(C14 - C16) with the stabilization energies of 19.01, 19.18, 19.60, 19.77, 18.81, 19.74, 20.46 and 20.44 kcal/mol respectively. The stabilization energy values associated with hyperconjugative interactions were LP(2) O20 to π*(C14 - C16) was 26.19 kcal/mol, LP(2) O22 to π*(C9 - C11) was 29.17 kcal/mol, LP(2) O24 to π*(C10 - C12) was 26.69 kcal/mol, LP (2) O25 to π*(C17 - C18) was 27.08 kcal/mol and LP(2) O19 to their adjacent σ*(C1 - C3) and σ* (C3 - C5) were 17.47 and 19.24 kcal/mol respectively. All possible interactions along with their stabilization energies were presented in Table 9.

Non covalent interaction analysis

We proceeded to characterize the type of interaction that occurred in the system using the Multiwfn 3.8 program. NCI plots for this compound was generated with the plots of reduced density gradient RDG against sign (λ_2) ρas shown in Fig. 5. NCI index was a powerful means to study non covalent interactions[59]. It has been employed widely to study the strength and nature of interactions[60,61].

sign(λ_2)ρ> 0: repulsive/non-bonding interaction

sign(λ_2)ρ< 0: attractive interactions hydrogen bond

sign(λ_2)ρ ≈ 0: Van der Waals interaction

The interactions in this compound was further visualized by the gradient isosurface in real space of

Table 9 — Second order perturbation theory analysis of Fock matrix in NBO basis for the title molecule

Donor NBO (i)	Type	ED/e (a.u.)	Acceptor NBO (j)	Type	ED/e (a.u.)	E(2) kcal/mol	E(j)-E(i) a.u.	F(i,j) a.u.
C1 - H28	σ	1.96716	C3 - C5	σ*	0.07033	4.01	0.89	0.054
C2 - H29	σ	1.96056	N4 - C6	σ*	0.03398	4.51	0.82	0.054
C5 - H31	σ	1.94168	C3 - O19	π*	0.09001	6.68	0.50	0.052
C5 - H31	σ	1.94168	C6 - C7	σ*	0.04342	4.04	0.90	0.054
C6 - H32	σ	1.96252	C2 - N4	σ*	0.03267	4.51	0.82	0.054
C6 - H32	σ	1.96252	C7 - C8	σ*	0.02666	4.03	1.06	0.059
C7 - C8	σ	1.97157	C7 - C9	σ*	0.02215	4.05	1.25	0.064
C7 - C8	π	1.68628	N4 - C6	σ*	0.03398	4.55	0.59	0.050
C7 - C8	π	1.68628	C9 - C11	π*	0.39802	19.01	0.27	0.065
C7 - C8	π	1.68628	C10 - C12	π*	0.38439	19.18	0.27	0.066
C7 - C9	σ	1.96651	C7 - C8	σ*	0.02666	4.02	1.26	0.064
C7 - C9	σ	1.96651	C11 - O22	σ*	0.02804	4.14	1.03	0.059
C8 - C10	σ	1.97332	C7 - C8	σ*	0.02666	4.08	1.27	0.064
C8 - H33	σ	1.97676	C7 - C9	σ*	0.02215	4.54	1.07	0.062
C9 - C11	σ	1.97603	C7 - C9	σ*	0.02215	4.18	1.27	0.065
C9 - C11	σ	1.97603	C11 - C12	σ*	0.03467	4.72	1.25	0.069
C9 - C11	π	1.70132	C7 - C8	π*	0.36513	18.73	0.30	0.068
C9 - C11	π	1.70132	C10 - C12	π*	0.38439	19.54	0.29	0.069
C9 - H34	σ	1.97525	C7 - C8	σ*	0.02666	4.47	1.11	0.063
C10 - C12	σ	1.97620	C11 - C12	σ*	0.03467	4.67	1.25	0.068
C10 - C12	σ	1.97620	C11 - O22	σ*	0.02804	2.96	1.06	0.050
C10 - C12	π	1.68585	C7 - C8	π*	0.36513	19.93	0.30	0.070
C10 - C12	π	1.68585	C9 - C11	π*	0.39802	19.25	0.28	0.067
C10 - H35	σ	1.97697	C7 - C8	σ*	0.02666	4.12	1.11	0.060
C10 - H35	σ	1.97697	C11 - C12	σ*	0.03467	4.15	1.07	0.060
C11 - C12	σ	1.96805	C9 - C11	σ*	0.02532	4.40	1.26	0.067
C11 - C12	σ	1.96805	C10 - C12	σ*	0.02386	4.37	1.27	0.067
C13 - C14	σ	1.96730	C14 - C16	σ*	0.02758	4.25	1.24	0.065
C13 - C14	σ	1.96730	C16 - O20	σ*	0.03011	4.66	1.02	0.062
C13 - C15	π	1.67966	C14 - C16	π*	0.41067	19.60	0.27	0.066
C13 - C15	π	1.67966	C17 - C18	π*	0.38449	19.77	0.28	0.067
C14 - C16	σ	1.97501	C13 - C14	σ*	0.02503	4.44	1.28	0.067
C14 - C16	σ	1.97501	C16 - C18	σ*	0.03799	5.19	1.25	0.072
C14 - C16	π	1.69663	C13 - C15	π*	0.38087	18.81	0.30	0.068
C14 - C16	π	1.69663	C17 - C18	π*	0.38449	19.74	0.30	0.070
C14 - H36	σ	1.97384	C13 - C15	σ*	0.02312	4.39	1.09	0.062
C14 - H36	σ	1.97384	C16 - C18	σ*	0.03799	4.01	1.07	0.059
C15 - H37	σ	1.97881	C13 - C14	σ*	0.02503	4.52	1.08	0.063
C16 - C18	σ	1.97065	C14 - C16	σ*	0.02758	4.87	1.27	0.070
C16 - C18	σ	1.97065	C17 - C18	σ*	0.02285	4.83	1.29	0.070
C17 - C18	σ	1.97343	C16 - C18	σ*	0.03799	4.72	1.25	0.069
C17 - C18	π	1.65725	C13 - C15	π*	0.38087	20.46	0.29	0.070
C17 - C18	π	1.65725	C14 - C16	π*	0.41067	20.44	0.28	0.069
C17 - H38	σ	1.97602	C13 - C15	σ*	0.02312	4.11	1.08	0.059
C17 - H38	σ	1.97602	C16 - C18	σ*	0.03799	4.46	1.06	0.062
C23 - H42	σ	1.99050	C11 - O22	σ*	0.02804	4.05	0.89	0.054
O24 - H45	σ	1.98728	C11 - C12	σ*	0.03467	4.59	1.28	0.069
O25 - H46	σ	1.98749	C17 - C18	σ*	0.02285	4.77	1.29	0.070
C26 - H49	σ	1.98629	C5 - C6	σ*	0.02974	4.08	0.86	0.053
N4	LP (1)	1.91067	C2 - C13	σ*	0.04299	7.55	0.70	0.065
N4	LP (1)	1.91067	C6 - C7	σ*	0.04342	6.98	0.70	0.063
O19	LP (2)	1.90061	C1 - C3	σ*	0.06214	17.47	0.66	0.097
O19	LP (2)	1.90061	C3 - C5	σ*	0.07033	19.24	0.67	0.102

(*Contd.*)

Table 9 — Second order perturbation theory analysis of Fock matrix in NBO basis for the title molecule (*Contd.*)

Donor NBO (i)	Type	ED/e (a.u.)	Acceptor NBO (j)	Type	ED/e (a.u.)	E(2) kcal/mol	E(j)-E(i) a.u.	F(i,j) a.u.
O20	LP (2)	1.86313	C14 - C16	π*	0.41067	26.19	0.35	0.093
O20	LP (2)	1.86313	C21 - H40	σ*	0.01810	5.44	0.70	0.057
O20	LP (2)	1.86313	C21 - H41	σ*	0.01834	5.52	0.70	0.057
O22	LP (1)	1.96258	C9 - C11	σ*	0.02532	7.04	1.10	0.079
O22	LP (2)	1.84556	C9 - C11	π*	0.39802	29.17	0.34	0.094
O22	LP (2)	1.84556	C23 - H43	σ*	0.01974	5.67	0.69	0.058
O22	LP (2)	1.84556	C23 - H44	σ*	0.02008	5.90	0.69	0.059
O24	LP (1)	1.98215	C10 - C12	σ*	0.02386	5.33	1.16	0.070
O24	LP (2)	1.87750	C10 - C12	π*	0.38439	26.69	0.34	0.092
O25	LP (1)	1.97913	C16 - C18	σ*	0.03799	5.92	1.16	0.074
O25	LP (2)	1.87384	C17 - C18	π*	0.38449	27.08	0.35	0.093
C9 - C11	π*	0.39802	C7 - C8	π*	0.36513	164.45	0.02	0.079
C10 - C12	π*	0.38439	C7 - C8	π*	0.36513	213.71	0.01	0.080
C14 - C16	π*	0.41067	C13 - C15	π*	0.38087	244.81	0.01	0.081

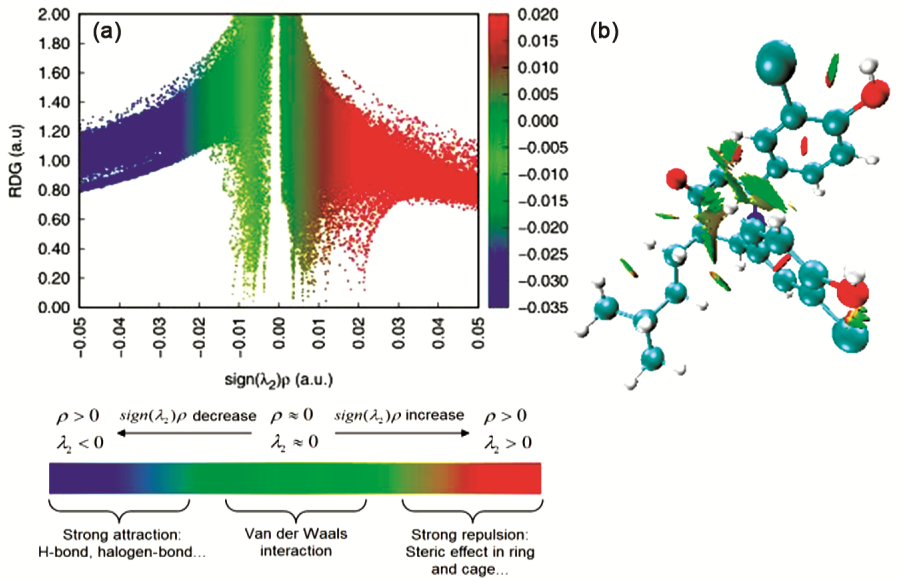

Fig. 5 — (a) Non covalent interaction and (b) isosurface of the title molecule

the molecules by using VMD 1.9.3 tool and shown in Fig. 5. In this 3-D visualization- the color coding was assigned to three different colors- namely- blue for attractive- red for repulsive and green for intermediate interactions[62]. The characteristic spikes at negative indicating the presence of non-covalent interactions- whereas peaks at positive indicating repulsive and the peaks nearer to zero indicating Van der Waals interaction 1. The interaction gets stronger when the spike moves further away from zero. The plot of RDG against sign $(\lambda_2)\rho$ will be useful in understanding the nature and strength of interactions. The interaction was attractive if $(\lambda_2)\rho < 0$ and the interaction was repulsive if $(\lambda_2)\rho > 0$. The RDG analysis was carried out at isosurface value of 0.5. The pictorial representation of RDG isosurface was obtained using multiwfn 3.8 and VMD 1.9.3 software (Fig. 5). The RDG isosurface interactions appear at bond and ring critical points. For the compound, the regions at the center of the two six membered rings correspond to strong steric interaction or the repulsive interactions, since they were filled by red sphere. The formation of a ring due to hydrogen bonding interaction was further confirmed by the presence of repulsive ring critical point in the isosurface. The interaction region marked by green sphere can be identified as Van der Waals interaction region, because the mapped color was green or light brown, which shows that the electron density in this region was low.

Topology analyses with ELF and LOL analysis

Shaded Map Surface with projection effect of electron localization function (ELF)

The topological analyses of the electron localization function ELF and the localized orbital locator LOL were completed using Multiwfn 3.8 program. LOL and ELF share a similar interpretation depending on the kinetic energy density[63]. Color shade map of the ELF and LOL for the title molecule were presented in Fig. 6(a) and Fig. 6(b).

From Fig. 6(a), the high ELF regions were seen around hydrogen atoms indicating the presence of highly localized bonding and nonbonding electrons. The blue regions around few carbon atoms show the delocalized electron cloud around it.

From the Fig. 6(b), it was seen that the central region of a hydrogen atom was white, indicates that electron density exceeds the upper limit of color scale 0.80. The covalent regions were seen between hydrogen and nitrogen atoms, indicated by red color with high LOL value, the electron depletion regions between valence shell and inner shell were shown by the blue circles around the carbon and oxygen nuclei. In general, a large ELF or LOL value[64] in a region indicates high localization of electrons due to the presence of a covalent bond, a lone pair of electrons or a nuclear shell in that region[65].

The covalent regions were seen between hydrogen and nitrogen atoms- indicated by red color with high LOL value, the electron depletion regions between valence shell and inner shell were shown by the blue circles around the carbon and oxygen nuclei. LOL conveys a more decisive and clearer picture than ELF[66].

Vibrational assignments

The vibrational wavenumbers and suitable description of each normal modes were determined by DFT/B3LYP method using 6-311G(d,p) basis set for the title compound and the results were compared with the experimental values and were presented in Table 10. Furthermore to the three translational and three rotational degrees of freedom, the maximum number of potentially active normal modes of vibrations of a nonlinear molecule that contains N

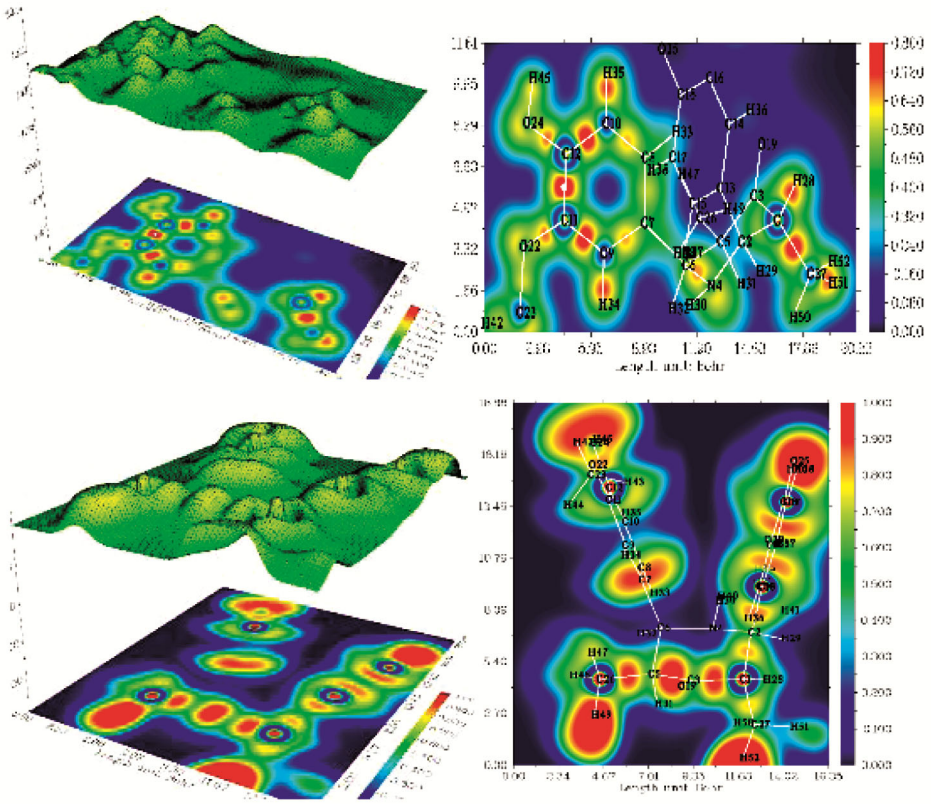

(a) Colur filled ELF (b) Colur filled with LOL

Fig. 6

Table 10 — Vibrational wave numbers obtained for the target molecule at B3LYP/6-311G (d,p) level of theory

Modes	Experimental Frequency (cm^{-1})	6-311G(d,p)	Scaled	I_{IR} (km mol^{-1})	strength	Assignments with PED
150		3743	3616	56.1638	m	$\nu O^{24}H^{45}$ (100)
149	3505	3649	3525	82.4308	m	$\nu O^{25}H^{46}$ (100)
148		3473	3355	0.5804	vw	$\nu N^{4}H^{30}$ (100)
147		3186	3078	1.5762	vw	$\nu C^{14}H^{36}$ (99)
146		3167	3059	6.1099	vw	$\nu C^{17}H^{38}$ (94)
145		3164	3057	6.7137	vw	$\nu C^{8}H^{33}$ (51), $\nu C^{10}H^{35}$ (48)
144		3155	3047	6.7076	vw	$\nu C^{9}H^{34}$ (98)
143		3148	3041	9.6899	vw	$\nu C^{8}H^{33}$ (47), $\nu C^{10}H^{35}$ (52)
142		3130	3023	11.6596	w	$\nu C^{15}H^{37}$ (95)
141		3101	2996	17.2157	w	$\nu_{asym}C^{26}H^{47}$ (79), $\nu_{asym}C^{26}H^{48}$ (18)
140		3089	2984	28.8160	w	ν $C^{23}H^{42}$ (90)
139		3081	2976	28.3135	w	$\nu_{asym}C^{27}H^{50}$ (64), $\nu_{asym}C^{27}H^{51}$ (16)
138		3080	2975	26.4351	w	$\nu_{asym}C^{21}H^{40}$ (48), $\nu_{asym}C^{21}H^{41}$ (45)
137		3079	2974	28.4507	w	$\nu C^{21}H^{39}$ (82)
136		3072	2968	33.8046	w	$\nu_{asym}C^{26}H^{48}$ (42), $\nu_{asym}C^{26}H^{49}$ (47)
135		3071	2967	17.6943	w	$\nu_{asym}C^{27}H^{51}$ (41), $\nu_{asym}C^{27}H^{52}$ (51)
134		3065	2961	41.8015	w	$\nu_{asym}C^{23}H^{43}$ (47), $\nu_{asym}C^{23}H^{44}$ (53)
133		3038	2934	4.8711	vw	$\nu C^{17}H^{38}$ (93)
132		3021	2918	28.2554	w	$\nu_{sym}C^{26}H^{47}$ (16), $\nu_{sym}C^{26}H^{48}$ (36), $\nu_{sym}C^{26}H^{49}$ (45)
131		3012	2909	36.5542	w	$\nu_{sym}C^{27}H^{50}$ (24), $\nu_{sym}C^{27}H^{51}$ (37), $\nu_{sym}C^{27}H^{52}$ (36)
130		3005	2903	39.0697	w	$\nu_{sym}C^{21}H^{39}$ (17), $\nu_{sym}C^{21}H^{40}$ (41), $\nu_{sym}C^{21}H^{41}$ (41)
129		3002	2900	6.6560	vw	$\nu C^{5}H^{31}$ (92)
128		2997	2895	49.8878	w	$\nu_{sym}C^{23}H^{42}$ (10), $\nu_{sym}C^{23}H^{43}$ (49), $\nu_{sym}C^{23}H^{44}$ (41)
127		2961	2860	27.2956	w	$\nu C^{2}H^{29}$ (86), $\nu C^{6}H^{32}$ (13)
126		2958	2857	45.7850	w	$\nu C^{2}H^{29}$ (13), $\nu C^{6}H^{32}$ (85)
125	1716.11	1681	1624	118.0182	s	$\nu O^{19}C^{3}$ (88)
124	1636.63	1656	1600	38.9018	w	$\nu C^{17}C^{18}$ (22), $\nu C^{18}C^{16}$ (17), $\nu C^{13}C^{14}$ (11), $\beta H^{46}O^{25}C^{18}$ (10)
123		1653	1597	18.6340	w	$\nu C^{8}C^{7}$ (20), $\nu C^{11}C^{12}$ (23)
122		1631	1576	39.8318	w	$\nu C^{15}C^{17}$ (29), $\nu C^{18}C^{16}$ (22)
121	1517.57	1618	1563	46.6042	w	$\nu C^{12}C^{10}$ (23), $\nu C^{9}C^{11}$ (19), $\beta C^{9}C^{11}C^{12}$ (14)
120		1549	1496	183.9015	s	$\beta H^{33}C^{8}C^{10}$ (11), $\beta H^{34}C^{9}C^{7}$ (10), $\beta H^{35}C^{10}C^{8}$ (15)
119		1546	1494	94.8703	m	$\beta H^{36}C^{14}C^{16}$ (18), $\beta H^{38}C^{17}C^{18}$ (10)
118	1465.69	1516	1465	7.7475	vw	$\rho H^{50}C^{27}H^{52}$ (24), $\rho H^{51}C^{27}H^{50}$ (45), $\tau H^{50}C^{27}C^{1}C^{2}$ (10)
117		1514	1462	15.8117	w	$\beta H^{30}N^{4}C^{6}$ (48), $\tau H^{30}N^{4}C^{6}C^{5}$ (10)
116		1509	1458	9.1487	vw	$\rho H^{47}C^{26}H^{49}$ (52), $\rho H^{49}C^{26}H^{48}$ (11), $\tau H^{49}C^{26}C^{5}C^{6}$ (12)
115		1508	1457	10.0339	w	$\rho H^{39}C^{21}H^{41}$ (45), $\rho H^{40}C^{21}H^{39}$ (32), $\tau H^{39}C^{21}O^{20}C^{16}$ (14)
114		1505	1454	8.3710	vw	$\rho H^{42}C^{23}H^{44}$ (45), $\rho H^{43}C^{23}H^{42}$ (33), $\tau H^{42}O^{23}C^{22}C^{11}$ (14)
113		1501	1450	13.3628	w	$\rho H^{50}C^{27}H^{52}$ (15), t $H^{51}C^{27}H^{50}$ (48), $\tau H^{52}C^{27}C^{1}C^{2}$ (12)
112		1498	1447	29.9095	w	$\rho H^{39}C^{21}H^{41}$ (19), t $H^{40}C^{21}H^{39}$ (29), $\rho H^{41}C^{21}H^{40}$ (26), $\tau H^{40}C^{21}O^{20}C^{16}$ (11)
111		1494	1443	31.4675	w	t $H^{42}C^{23}H^{44}$ (12), t $H^{43}C^{23}H^{42}$ (22), $\rho H^{44}C^{23}H^{43}$ (43), $\tau H^{43}C^{23}O^{22}C^{11}$ (12)
110		1493	1442	6.3837	vw	$\rho H^{48}C^{26}H^{47}$ (42), $\rho H^{49}C^{26}H^{48}$ (33), $\tau H^{48}C^{26}C^{5}C^{6}$ (14)
109		1490	1439	29.9429	w	$\rho H^{39}C^{21}H^{41}$ (10), $\omega H^{40}C^{21}H^{39}$ (12), $\rho H^{41}C^{21}H^{40}$ (53)
108		1484	1433	7.2344	vw	$\omega H^{42}C^{23}H^{44}$ (19), $\omega H^{43}C^{23}H^{42}$ (21), $\rho H^{44}C^{23}H^{43}$ (43)
107	1413.94	1463	1414	31.4783	w	$\nu C^{13}C^{14}$ (12), $\beta H^{46}O^{25}C^{18}$ (17)
106		1454	1405	11.1118	w	$\beta H^{33}C^{8}C^{10}$ (14), $\beta H^{32}C^{6}C^{7}$ (22)
105	1384.46	1433	1384	7.8577	vw	$\omega H^{47}C^{26}H^{49}$ (22), $\omega H^{48}C^{26}H^{47}$ (33), $\omega H^{49}C^{26}H^{48}$ (38)
104		1420	1372	7.4687	vw	$\omega H^{50}C^{27}H^{52}$ (37), $\omega H^{51}C^{27}H^{50}$ (25), $\omega H^{51}C^{27}H^{50}$ (28)
103		1416	1368	79.2853	m	$\nu C^{14}C^{16}$ (10), $\beta H^{46}O^{25}C^{18}$ (35), $\beta H^{37}C^{15}C^{17}$ (21)
102		1403	1355	26.0673	w	$\nu C^{9}C^{11}$ (10), $\beta H^{31}C^{2}C^{26}$ (17), $\beta H^{32}C^{6}C^{7}$ (19), $\tau H^{32}C^{6}C^{7}C^{8}$ (12)
101		1389	1342	7.6237	vw	$\beta H^{28}C^{1}C^{27}$ (13), $\beta H^{29}C^{2}N^{4}$ (11), $\tau H^{29}C^{2}C^{13}C^{14}$ (31)
100		1383	1336	33.5143	w	$\beta H^{45}O^{24}C^{12}$ (12), $\beta H^{32}C^{6}C^{7}$ (14), $\tau H^{32}C^{6}C^{7}C^{8}$ (12)
99		1377	1330	30.9709	w	$\beta H^{29}C^{2}N^{4}$ (38), $\tau H^{28}C^{1}C^{3}C^{5}$ (15), $\tau H^{29}C^{2}C^{13}C^{14}$ (11)

(*Contd.*)

Table 10 — Vibrational wave numbers obtained for the target molecule at B3LYP/6-311G (d,p) level of theory (*Contd*.)

Modes	Experimental Frequency (cm^{-1})	6-311G(d,p)	Scaled	I_{IR} (km mol^{-1})	strength	Assignments with PED
98		1368	1321	106.5469	s	$\beta H^{45}O^{24}C^{12}$ (20), $\beta H^{32}C^{6}C^{7}$ (21)
97		1352	1306	5.0362	vw	$\beta H^{28}C^{1}C^{27}$ (15), $\beta H^{29}C^{2}N^{4}$ (21), $\tau H^{28}C^{1}C^{3}C^{5}$ (18)
96	1293.28	1331	1286	21.1154	w	$\beta H^{28}C^{1}C^{27}$ (31), $\beta H^{31}C^{2}C^{26}$ (12), $\tau H^{32}C^{6}C^{7}C^{8}$ (11),
95		1325	1279	9.1130	vw	$\nu C^{8}C^{7}$ (10), $\tau H^{31}C^{5}C^{3}C^{1}$ (22)
94	1263.10	1313	1269	84.7697	m	$\nu C^{14}C^{16}$ (10), $\nu O^{20}C^{16}$ (13), $\rho H^{36}C^{14}C^{16}$ (32)
93		1298	1254	134.7967	s	$\nu O^{24}C^{12}$ (10)
92	1245.51	1294	1250	80.8139	m	$\nu O^{24}C^{12}$ (24), $\beta H^{35}C^{10}C^{8}$ (10)
91		1284	1240	54.7923	m	$\nu C^{15}C^{17}$ (12), $\nu C^{13}C^{14}$ (31)
90	1229.38	1277	1234	145.1060	s	$\nu C^{17}C^{18}$ (11), $\nu O^{25}C^{18}$ (27), $\beta H^{46}O^{25}C^{18}$ (17), $\beta H^{37}C^{15}C^{17}$ (16), $\beta H^{38}C^{17}C^{18}$ (10)
89		1262	1219	103.7729	s	$\nu O^{22}C^{11}$ (13)
88		1249	1207	31.9540	w	$\tau H^{31}C^{5}C^{3}C^{1}$ (15)
87		1241	1199	48.7288	w	$\tau H^{31}C^{5}C^{3}C^{1}$ (10)
86	1186.48	1221	1180	62.1357	m	$\beta H^{45}O^{24}C^{12}$ (19), $\beta H^{34}C^{9}C^{7}$ (19)
85		1215	1174	40.9250	w	$\beta H^{32}C^{6}N^{4}$ (15)
84	1161.00	1206	1165	20.6589	w	$\tau H^{43}C^{23}O^{22}C^{11}$ (16), $\tau H^{44}C^{23}O^{22}C^{11}$ (20)
83		1199	1158	0.6961	vw	t $H^{41}C^{21}H^{40}$ (12), r $H^{39}C^{21}H^{40}$ (12), $\tau H^{40}C^{21}O^{20}C^{16}$ (28), $\tau H^{41}C^{21}O^{20}C^{16}$ (28)
82		1186	1146	40.3076	w	$\beta H^{35}C^{10}C^{8}$ (11), $\tau H^{43}C^{23}O^{22}C^{11}$ (13), $\tau H^{44}C^{23}O^{22}C^{11}$ (14)
81		1178	1138	1.1487	vw	r $H^{39}C^{21}H^{41}$ (11), r $H^{40}C^{21}H^{41}$ (32), $\tau H^{39}C^{21}O^{20}C^{16}$ (28), $\tau H^{40}C^{21}O^{20}C^{16}$ (12)
80		1178	1138	0.7042	vw	r $H^{43}C^{23}H^{44}$ (10), $\tau H^{42}C^{23}O^{22}C^{11}$ (28), $\tau H^{43}C^{23}O^{22}C^{11}$ (14)
79		1173	1133	32.4456	w	$\nu C^{2}C^{13}$ (10), $\rho H^{38}C^{17}C^{18}$ (11)
78	1127.05	1166	1126	48.5428	w	$\nu C^{2}C^{13}$ (10)
77		1160	1121	107.4064	s	$\nu C^{10}C^{8}$ (10), $\beta H^{33}C^{8}C^{10}$ (10)
76		1148	1109	27.1940	w	$\nu C^{15}C^{17}$ (12), $\beta C^{15}C^{17}C^{18}$ (12), $\beta H^{37}C^{15}C^{17}$ (21), $\beta H^{38}C^{17}C^{18}$ (14)
75		1142	1104	24.0118	w	$\nu C^{26}C^{5}$ (13)
74		1123	1084	11.5348	w	$\tau H^{31}C^{5}C^{3}C^{1}$ (10), $\tau H^{47}C^{26}C^{5}C^{6}$ (10)
73		1091	1054	12.0389	w	$\nu C^{27}C^{1}$ (34)
72	1032.20	1067	1031	3.2950	vw	$\nu N^{4}C^{6}$ (18)
71		1061	1025	33.8582	w	$\nu O^{22}C^{23}$ (57), $\beta C^{9}C^{11}C^{12}$ (14), $\beta C^{12}C^{10}C^{8}$ (10)
70		1059	1023	62.7869	m	$\nu O^{20}C^{21}$ (52), $\beta C^{15}O^{17}C^{18}$ (14), $\beta C^{14}C^{16}C^{18}$ (12)
69	1014.97	1049	1014	14.6405	w	$\tau H^{48}C^{26}C^{5}C^{6}$ (15)
68	983.04	1025	990	2.5614	vw	$\nu C^{27}C^{1}$ (14), $\tau H^{49}C^{26}C^{5}C^{6}$ (10)
67		1000	966	18.7427	w	$\tau H^{50}C^{27}C^{1}C^{2}$ (11), $\tau H^{52}C^{27}C^{1}C^{2}$ (19)
66	938.72	963	930	5.2053	vw	$\tau H^{33}C^{8}C^{7}C^{6}$ (41)
65		955	923	6.5692	vw	$\tau H^{33}C^{8}C^{7}C^{6}$ (34)
64		948	916	2.9137	vw	$\nu C^{2}C^{13}$ (12)
63		944	911	0.6019	vw	$\tau H^{37}C^{15}C^{17}C^{18}$ (31), $\tau H^{38}C^{17}C^{18}C^{16}$ (36)
62		922	891	13.5901	w	$\gamma H^{36}C^{14}C^{16}C^{18}$ (12)
61		895	865	31.2041	w	$\gamma H^{36}C^{14}C^{16}C^{18}$ (48)
60		889	859	5.1556	vw	$\gamma H^{36}C^{14}C^{16}C^{18}$ (32)
59	849.04	872	842	23.2663	w	$\gamma H^{34}C^{9}C^{7}C^{6}$ (72)
58	835.21	865	836	11.7531	w	$\gamma H^{38}N^{4}C^{6}$ (20)
57	823.02	836	807	18.2070	w	$\tau H^{37}C^{15}C^{17}C^{18}$ (32), $\tau H^{38}C^{17}C^{18}C^{16}$ (30)
56	797.69	827	799	22.4546	w	$\nu O^{25}C^{18}$ (10)
55		809	782	30.9764	w	$\tau H^{35}C^{10}C^{8}C^{7}$ (10)
54		800	773	37.6641	w	$\tau H^{33}C^{8}C^{7}C^{6}$ (10), $\tau H^{35}C^{10}C^{8}C^{7}$ (53)
53		795	768	67.0530	m	$\nu C^{9}C^{11}$ (14), $\nu C^{11}C^{12}$ (21), $\nu O^{24}C^{12}$ (13), $\nu O^{22}C^{11}$ (10)
52		767	741	11.7470	w	$\tau H^{37}C^{15}C^{17}C^{18}$ (20)
51		744	719	5.3208	vw	$\tau C^{12}C^{10}C^{8}C^{7}$ (19), $\tau C^{11}C^{12}C^{10}C^{8}$ (11), $\gamma O^{19}C^{1}C^{5}C^{3}$ (10)
50		717	693	1.4393	vw	$\tau C^{17}C^{18}C^{16}C^{14}$ (17), $\tau C^{15}C^{17}C^{18}C^{16}$ (16), $\tau C^{13}C^{14}C^{16}C^{18}$ (24), $\gamma O^{25}C^{16}C^{17}C^{18}$ (12)
49		712	688	0.8712	vw	$\tau C^{12}C^{10}C^{8}C^{7}$ (11), $\tau C^{9}C^{11}C^{12}C^{10}$ (12), $\tau C^{11}C^{12}C^{10}C^{8}$ (11), $\gamma O^{24}C^{10}C^{11}C^{12}$ (14), $\gamma O^{22}C^{12}C^{9}C^{11}$ (16)

(*Contd*.)

Table 10 — Vibrational wave numbers obtained for the target molecule at B3LYP/6-311G (d,p) level of theory (*Contd*.)

Modes	Experimental Frequency (cm^{-1})	6-311G(d,p)	Scaled	I_{IR} (km mol^{-1})	strength	Assignments with PED
48	663.18	705	681	39.3883	w	νC^3C^5 (13), $\tau H^{30}N^4C^6C^5$ (12)
47		666	643	16.4802	w	$\tau H^{30}N^4C^6C^5$ (10)
46	627.57	660	638	9.1844	vw	$\tau C^{12}C^{10}C^8C^7$ (10), $\tau C^9C^{11}C^{12}C^{10}$ (10), $\gamma O^{22}C^{12}C^9C^{11}$ (15)
45		635	613	19.5758	w	$\tau H^{30}N^4C^6C^5$ (15)
44		624	603	6.4165	vw	$\tau H^{33}C^8C^{10}C^{12}$ (10)
43		604	583	82.0903	m	$\tau H^{46}O^{25}C^{18}C^{16}$ (94)
42		585	566	6.5238	vw	$\beta O^{25}C^{18}C^{17}$ (14)
41	556.52	581	562	7.0630	vw	$\rho O^{19}C^3C^5$ (18)
40	539.76	566	546	4.2974	vw	$\beta O^{24}C^{12}C^{10}$ (21)
39		548	529	1.0493	vw	$\beta O^{19}C^3C^5$ (14), $\beta C^{24}C^{12}C^{10}$ (11)
38		528	510	1.9715	vw	$\beta C^{11}O^{22}C^{23}$ (11), $\beta C^{11}C^{12}C^{10}$ (13)
37		525	507	3.3168	vw	$\beta C^{17}C^{18}C^{16}$ (16), $\beta C^{21}O^{20}C^{16}$ (24)
36		490	473	2.0393	vw	$\tau H^{35}C^{10}C^8C^7$ (10)
35		478	462	8.1252	vw	$\tau C^{12}C^{10}C^8C^7$ (10), $\tau C^{11}C^{12}C^{10}C^8$ (14), $\gamma O^{24}C^{10}C^{11}C^{12}$ (15), $\gamma O^{22}C^{12}C^9C^{11}$ (12)
34		470	454	5.4620	vw	$\tau H^{36}C^{14}C^{16}C^{18}$ (10), $\tau H^{38}C^{17}C^{18}C^{16}$ (11), $\tau C^{15}C^{17}C^{18}C^{16}$ (22), $\gamma O^{25}C^{16}C^{17}C^{18}$ (17), $\gamma O^{20}C^{14}C^{18}C^{16}$ (21)
33		453	438	13.9114	w	$\gamma C^7C^6N^4$ (10)
32		440	425	9.8486	vw	$\gamma N^4C^2C^{13}$ (11), $\gamma O^{25}C^{16}C^{17}C^{18}$ (11)
31		438	423	89.7233	m	$\tau H^{45}O^{24}C^{12}C^{10}$ (90)
30		414	400	7.1023	vw	$\tau C^7C^6N^4C^2$ (10)
29		386	373	1.6635	vw	$\gamma O^{24}C^{10}C^{11}C^{12}$ (14), $\gamma C^{26}C^6C^3C^5$ (12)
28		358	346	1.7455	vw	$\gamma O^{25}C^{18}C^{17}$ (14), $\gamma C^{21}O^{20}C^{16}$ (16)
27		354	342	1.5341	vw	$\gamma C^{11}O^{22}C^{23}$ (30), $\gamma O^{24}C^{12}C^{10}$ (16)
26		331	320	3.0021	vw	$\gamma C^{25}C^{18}C^{16}$ (11)
25		312	302	0.8346	vw	$\beta C^{26}C^5C^3$ (12), $\tau H^{39}C^{21}O^{20}C^{16}$ (10)
24		308	297	7.1818	vw	$\gamma C^{26}C^5C^3$ (12)
23		291	281	3.3419	vw	$\tau H^{39}C^{21}O^{20}C^{16}$ (12)
22		280	271	0.8255	vw	$\tau H^{42}C^{23}O^{22}C^{11}$ (19)
21		275	266	0.3231	vw	$\gamma C^{26}C^5C^3$ (26)
20		267	258	0.3292	vw	$\tau H^{50}C^{27}C^1C^2$ (24), $\tau H^{52}C^{27}C^1C^2$ (13)
19		257	248	5.1321	vw	$\beta O^{22}C^{11}C^9$ (13), $\beta C^{26}C^5C^3$ (13)
18		233	225	0.3759	vw	$\gamma C^{27}C^1C^3$ (29)
17		230	223	1.2983	vw	$\tau H^{41}C^{21}C^{20}C^{15}$ (12)
16		223	216	0.5352	vw	$\beta O^{20}C^{16}C^{18}$ (13), $\gamma C^{27}C^1C^3$ (16), $\tau H^{48}C^{26}C^5C^6$ (10)
15		204	197	0.5618	vw	$\tau C^9C^{11}C^{12}C^{10}$ (10), $\gamma O^{22}C^{12}C^9C^{11}$ (12)
14		194	188	2.2420	vw	$\tau C^{27}C^1C^2N^4$ (13)
13		186	180	0.0097	vw	$\gamma C^7C^6N^4$ (14), $\tau C^8C^7C^6N^4$ (10), $\tau C^9C^{11}C^{12}C^{10}$ (26)
12		161	155	0.7722	vw	$\gamma C^2C^{13}C^{15}$ (11), $\gamma C^5C^6N^4$ (11)
11		143	139	0.6089	vw	$\gamma C^8C^7C^6$ (20), $\gamma O^{22}C^{11}C^9$ (16)
10		126	122	0.0767	vw	$\gamma C^8C^7C^6$ (18), $\tau C^{17}C^{18}C^{16}C^{14}$ (14)
9		118	114	1.9144	vw	$\tau C^2C^1C^3C^5$ (15)
8		107	103	4.9243	vw	$\tau C^{23}O^{22}C^{11}C^{12}$ (72)
7		99	96	3.0767	vw	$\tau C^{21}O^{20}C^{16}C^{14}$ (69)
6		98	95	3.2960	vw	$\rho C^2C^{13}C^{15}$ (22)
5		60	57	0.6831	vw	$\gamma C^7C^6N^4$ (10), $\tau C^{17}C^{18}C^{16}C^{14}$ (15), $\tau C^{10}C^8C^7C^6$ (22), $\gamma C^2C^{14}C^{15}C^{13}$ (14)
4		54	53	0.0023	vw	$\tau C^8C^7C^6N^4$ (35), $\tau C^{23}O^{22}C^{11}C^{12}$ (16)
3		48	47	1.6385	vw	$\tau C^{21}O^{20}C^{16}C^{14}$ (10), $\tau N^4O^2C^{13}C^{14}$ (46)
2		38	37	0.1457	vw	$\beta C^7C^6N^4$ (10), $\tau C^{10}C^8C^7C^6$ (13), $\tau C^6N^4C^2C^{13}$ (34)
1		25	24	0.0385	vw	$\beta N^4C^2C^{13}$ (11), $\tau C^8C^7C^6N^4$ (18), $\tau C^{10}C^8C^7C^6$ (11), $\tau N^4O^2C^{13}C^{14}$ (10), $\gamma C^2C^{14}C^{15}C^{13}$ (11)

ν, stretching; ν_s, symmetric stretching; ν_{as}, asymmteric stretching; β, in-plane bending; γ, out-of-plane bending; ω, wagging; r, rocking; t, twisting; ρ, scissoring, τ, torsion; I_{IR} (km mol^{-1}), IR intensities.

atoms was equal to (3N-6)[67]. The title compound consists of 52 atoms and so it has 150 normal modes of fundamental vibrations. The vibrational modes were assigned by comparing the computed results with that of experimental value. The calculated wave numbers were slightly overvalued than the experimental values for the majority of the normal modes. Two factors may be responsible for the

difference between the experimental and computed spectra of this compound. The first factor was a result of the environment and the second reason was due to the fact that the experimental value was an anharmonic wave number while the calculated value was a harmonic wave number. The theoretical wave numbers were in good agreement with experimental wave numbers after applying different scaling factors. In our present investigation, wave numbers in the ranges from 4000 cm^{-1} were scaled with an empirical scaling factor of 0.966 was used to improve the well-known systematic error caused by basis set incompleteness, neglect of electron correlation and vibrational anharmonicity[68]. The experimental and theoretical spectra were shown in Fig. 7.

C-H vibrations

The aromatic rings exhibit C–H stretching as well as in-plane and out-of-plane bending vibrations. The ring C-H stretching vibrations of aromatic and heteroaromatic structures generally occur in the region 3100–3000 cm^{-1} (Ref. 69). The intensities of each C-H stretching vibration mode were incredibly low. The calculated mode numbers (126–147) correspond to the C-H stretching bands. The benzene ring C-H in-plane bending vibrations were usually weak and observed in the region 1300–1000 cm^{-1} (Ref. 70), while the C-H out-of-plane bending vibrations lie in the region 900–650 cm^{-1} (Ref. 71). In the title compound, the bands at 849(w), 835(w) and 823(w) cm^{-1} were assigned in FT-IR to C-H out-of-plane bending vibrations and their calculated wave numbers were 842, 836 and 807 cm^{-1} respectively (mode no.59, 58, 57). The bands at 1384(vw), 1293(w), 1263(m), 1246(m), 1186(m), 1161(w) and 1015(w) cm^{-1} were due to C-H in-plane bending vibrations, which were in good agreement with the computed wavenumbers valued 1384, 1286, 1269, 1250,1180, 1165 and 1014 cm^{-1} (mode no. 105, 96, 94, 92, 86, 84, 69).

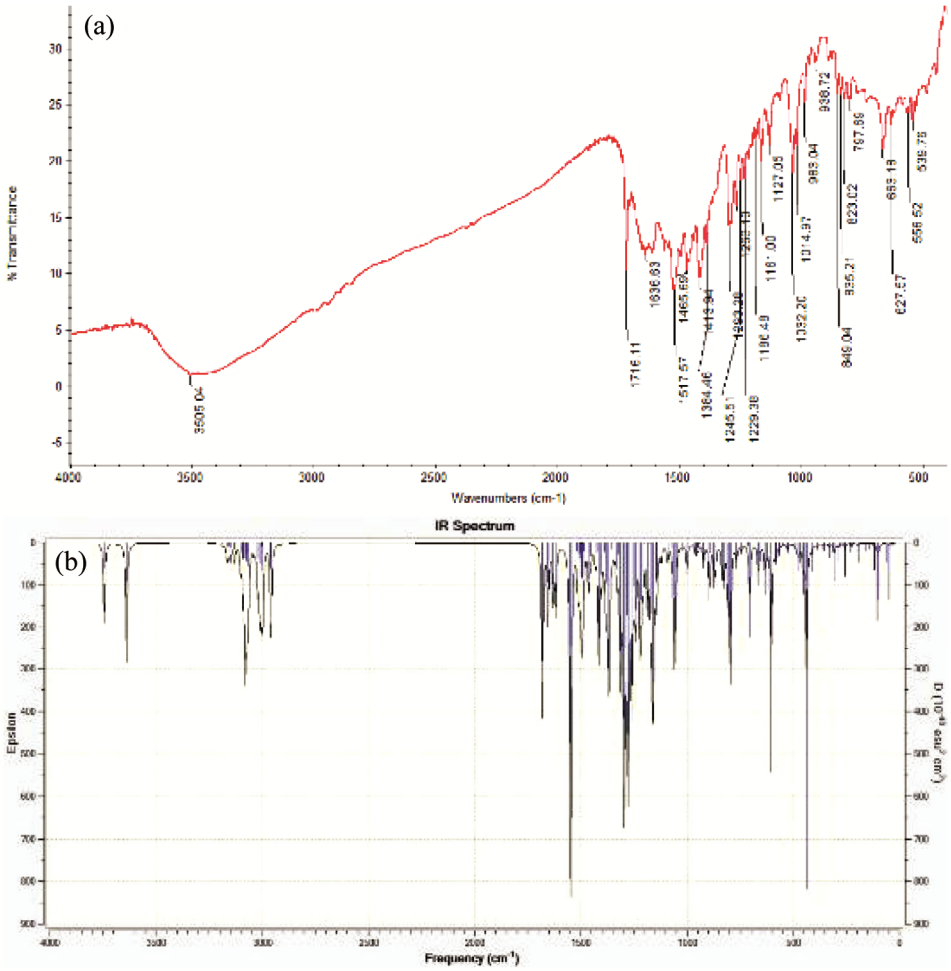

Fig. 7 — (a) Experimental (b) Simulated FT-IR spectra of BHMD by B3LYP/6-311G (d,p)

N–H vibrations

The N–H stretching vibration appears as a strong band within the region around 3500–3300 cm^{-1} (Ref. 72). In the current investigation, the title compound exhibited N4-H30 symmetric stretch at 3354 cm^{-1} (mode no. 3) by B3LYP method with 6-311G(d,p) level theory. It shows a positive deviation from the calculated value. It was due to the presence of strong hydrogen bonding in solid phase. As expected, this mode was purely a stretching mode, and was clear from the PED column also which has 100% contribution. The in-plane bending mode of H30–N4–C6 appeared at 1466 cm^{-1} (FT-IR) and its corresponding calculated wave number was 1462 cm^{-1} (mode no. 117) by B3LYP method with 6-311G(d,p) level of theory. It also possesses moderate PED contribution (48%).

O–H vibrations

The free hydroxyl group absorbs strongly in the region of 3700– 3584 cm^{-1}, whereas the existence of intermolecular hydrogen bond formation can lower the O–H stretching frequency in the range 3550–3200 cm^{-1} with increase in intensity and breadth[73]. In our present study, the band observed at 3505 cm^{-1} in FT-IR spectrum was assigned to O25–H46 stretching vibration, the calculated wavenumber for this mode was at 3525 cm^{-1} (mode no. 149) as shown in Table 10 shows deviation of about 82.4308cm^{-1} may be due to the presence of intermolecular hydrogen bonding. The expected PED for this mode was a pure mode of 100%. For O24-H45 the computed wave number was at 3616 cm^{-1} (mode no. 150) which has deviation of 56.1638cm^{-1} with 100% contribution in PED column. The O–H in-plane bending vibration in the phenol was generally typicaly ranges between the region 1150–1250 cm^{-1} and was significantly impacted due to hydrogen bonding unlike to stretching and out-of-plane bending frequencies[74]. In the present study the band at 1186, 1229 cm^{-1} in FT-IR spectrum was assigned to O24–H45 and O25–H46 in-plane bending vibration shows good correlation with computed wave number at 1180 and 1234 cm^{-1} respectively (mode no. 86 and 90).

C=O vibrations

The carbonyl stretching C=O vibration was expected to occur in the region 1715–1680 cm^{-1} (Ref. 75). In this study, we have observed C=O stretching in C3=O19 for the FT-IR spectrum at 1716(s) cm^{-1}, while the computed value was 1681 cm^{-1} (mode no. 125)and its PED value (88%).The deviation of the calculated wave numbers for this mode can be attributed to the underestimation of the large degree of p-electron delocalization of the molecule due to conjugation of the molecule[76].

C-N vibrations

The identification of C–N vibration was a very difficult task, since mixing of multiple bands were possible in this region. The ring C-C and C-N stretching vibrations occur in the wide range from 1640–900 cm^{-1} (Ref. 77). In the present investigation C–N stretching frequency was observed at 1032 cm^{-1} by FT-IR and their corresponding calculated wavenumber appeared in the range of 1031 cm^{-1} (mode no. 72). The experimental and theoretical parameters for the C-N stretching mode were in good agreement. The C–N stretching vibration normally appears around 1300 cm^{-1}. In this work the C–N frequencies were moderately lowered, which may be due to the mass effect around nitrogen atom[78].

C-C vibrations

The ring C-C stretching vibrations usually occur in the region 1650–1400 cm^{-1} (Ref. 79). The bonds tend to shift to slightly lower wave numbers with heavier substituents, and the more substituents on the ring, the wider the absorption zones. In the title molecule, the bonds observed in IR at 1637, 1518 and 1414 cm^{-1} were caused by the substituents in the benzene ring and have been attributed to C-C stretching. The calculated C–C stretching vibrations using B3LYP/ 6-311G (d,p) method were 1600, 1563 and 1414 cm^{-1} (mode no. 124,121,107). The corresponding ring in-plane bending vibrations were shown in Table 10. The ring deformation mode generally occurs in the region around 943– 923 cm^{-1} (Ref. 80). The bands at 1227(m), 698(m) and 600(w) cm^{-1} were assigned to ring torsion modes and their corresponding calculated values were 1224, 689 and 608 cm^{-1} (Ref. 81). These assignments were further supported well by the PED values.

O–CH_3 vibrations

Subramanian *et.al* have assigned O-CH_3strectching absorption in the region 3037–2915 cm^{-1} (Ref. 82). The vibrations in the methoxy group of bands were theoretically scaled by B3LYP/6-311G (d,p) method at 2984, 2975, 2974, 2961, 2903, 2895 cm^{-1} (mode no. 140, 138, 134, 130 and 128) were assigned to CH_3 asymmetric and symmetric stretching vibrations

respectively. The bending vibrations in the methoxy group of bands were calculated by B3LYP/6-311G(d,p) and the bands were found in 1457, 1454, 1447, 1443, 1439 and 1433 cm^{-1} (mode no. 115, 114, 112, 111, 109 and 108) were assigned to be bending vibrations such as twisting, scissoring, wagging respectively. In our title molecule this mode calculated at 281, 271 and 223 cm^{-1} were assigned to the O–CH_3 torsional mode.

Methyl group vibrations

The saturated hydrocarbon containing methyl group shows C-H stretching absorption bands in the region 3000–2840 cm^{-1} (Ref. 83). The computed values of (modes no.131, 132, 135, 136, 139 and 141) were attributed to methyl stretching vibrations and these values were also supported with the literature[84]. The out of plane bending vibrations of methyl group normally appear in the region 1465–1380 cm^{-1} (Ref. 85). The band at 1384(vw) cm^{-1} was attributed to wagging vibrations in FT-IR and its calculated value was 1384 cm^{-1} (mode no. 105). The other vibration values were calculated by B3LYP/6-311G(d,p) at 1442, 1450, 1458, 1465 cm^{-1} (mode no. 110, 113, 116 and 118).

Conclusion

In this present study of BHMD, the molecule was theoretically optimized using B3LYP with customary 6-311G (d,p) basis set. The bond distance, bond angle and dihedral angle were used to predict the geometry and stability of the atoms. Mulliken charge analysis was performed to distinguish the atoms which were electronegative and electropositive and also used to find the charge transfer takes place in the molecule. ESP was calculated to detect the electron rich and electron poor sites in the molecule. HOMO-LUMO and other quantum chemical parameter calculations were performed to expose the stability and hardness of the molecule. The NBO calculations explain the delocalisation, stabilization and hyperconjugation interaction of the molecule. From the NCI studies we conclude that the molecule has weak Van der Waals force and shows steric effect. By using the Multiwfn 3.8 software, the shaded surface map of BHMD facilitates to know the electron depletion area present in the molecule. The complete vibrational spectral analysis and theoretical calculation have been performed for BHMD molecule were completely assigned for the first time with the help of PED.

Acknowledgements

The authors would like to express their special thanks of gratitude to the Secretary and Principal of St. John's College, Palayamkottai, Tirunelveli 627 002, Tamil Nadu, India for providing the software and computer facilities.

References

1 Lima L L P D, Oliveira A Q T D, Moura T C F, Silva GraçaAmoras E D, Lima S S, Silva A N M R D, Queiroz M A F, Cayres-Vallinoto I M V, Ishak R & Vallinoto A C R, *Virology J*, 18 (2021) 78.
2 Hayes R J, Donnell D, Floyd S, Mandla N, Bwalya J, Sabapathy K & Fidler S, *New Eng J Med*, 381 (2019) 207.
3 Dybul M, Fauci A S, Bartlett J G, Kaplan J E & Pau A K, *Ann Intern Med*, 137 (2002) 381-433.
4 Hidaka K, Kimura T, Sankaranarayanan R, Wang J, McDaniel K F, Kempf D J, Kameoka M, Adachi M, Kuroki R, Nguyen J T, Hayashi Y & Kiso Y, *J Med Chem*, 61 (2018) 5138.
5 Harini S T, Kumar H V, Rangaswamy J, Naik N, *Russian J Bioorg Chem*, 43 (2017) 186.
6 De S, Banerjee S, Babu M N, Keerithi C N, *J Appl Pharm Res,* 3 (2015) 8.
7 Kuznetsov V V, Prostakov N S,*Chem Heterocy Com*, 30 (1994) 1.
8 Harini S T, Kumar H V, Rangaswamy J, Naik N, *Bioorg & Med Chem Lett,* 22 (24) (2012) 7588.
9 Fallah-Tafti A, Foroumadi A, Tiwari R, Shirazi A N, Hangauer D G, Bu Y, Akbarzadeh T, Parang K, Shafiee A, *Eur J Med Chem,* 46 (2011) 4853.
10 Yao B, Li N, WangC, Hou G, Meng Q, & Yan K, *Acta Cry Sec C Stru Chem*, 74 (2018) 659.
11 Selvendiran K, Tong L, Vishwanath S, Bratasz A, Trigg N J, Kutala V K, Kuppusamy P, *J Bio Chem*, 282 (2007) 28609.
12 Aridoss G, Amirthaganesan S, Ashok Kumar N, Kim J T, Lim, K T, Kabilan S, Jeong Y T, *Bioorg & Med Chem Lett*, 18 (2008) 6542.
13 Aridoss G, Parthiban P, Ramachandran R, Prakash M, Kabilan S, Jeong Y T, *Eur J Med Chem*, 44 (2009) 577.
14 Nithya P, Nawaz Khan F R, Roopan S, Shankar U & Jin J, *Chem Papers*, 65 (2011) 743.
15 Ganellin C R & Spickett R G W, *J Med Chem*, 8 (1965) 619.
16 Perumal R V, Adiraj M & Pandiyan P S, *Indian Drugs,* 38 (2001) 156.
17 Liu L, Liu S & Hou G, *Zeitschriftfür Kristallographie - New Cry Str,* 233 (2018) 1063.
18 Santelli-Rouvier C, Pradines B, Berthelot M, Parzy D & Barbe J, *Eur J MedChem*, 39 (2004) 735.
19 Bhattacharjee A K, Hartell M G, Nichols D A, Hicks R P, Stanton B, van Hamont J E & Milhous W K, *Eur J Med Chem*, 39 (2004) 59.
20 Verhaeghe P, Azas N, Gasquet M, Hutter S, Ducros C, Laget M & Vanelle P, *Bioorg & Med Chem Lett,* 18 (2008) 396.
21 Atwal K S, Swanson B N, Unger S E, Floyd D M, Moreland S, Hedberg A & O'Reilly B C, *J Med Chem,* 34 (1991) 806.
22 Wadood A, Ahmed N, Shah L, Ahmad A, Hassan H & Shams S, *OA Drug Design & Delivery*, 1 (2013) 1.

23 Baskaran C, Ramachandran M, *Asian Pac J Tro Dis*, 2 (2012) S734–S738.

24 Sussman J L, Lin D, Jiang J, Manning N O, Prilusky J, Ritter O & Abola E E, *Acta Crystallographica Sec D Bio Crys,* 54 (1998) 1078.

25 Discovery Studio Visualizer Software, Version 4.0, (2012). http://www.accelrys.com.

26 ACD/ChemSketch, Version 2020.1.2, (2020). Advanced Chemistry Development, Inc., Toronto, ON, Canada. www.acdlabs.com.

27 Noller C R, &Baliah V, *J Am Chem Soc,* 70 (1948) 3853.

28 Hanwell M D, Curtis D E, Lonie D C, Vandermeersch T, Zurek E & Hutchison G R, *J Cheminformatics*, 4 (2012) 1.

29 Dallakyan S & Olson A J, *Chem Bio*, (2014) 243.

30 Trott O, & Olson A J, *J Comp Chem*, 31 (2009) 455.

31 DeLano, W.L.(2002). The PyMOL Molecular Graphics System. Delano Scientific, San Carlos. CA, USA.

32 Frisch M J, Trucks G W, Schlegel H B, Scuseria G E, Robb M A, Cheeseman J R, Scalmani G, Barone V, Petersson G A, Nakatsuji H, Li X, Caricato M, Marenich A V, Bloino J, Janesko B G, Gomperts R, Mennucci B, Hratchian H P, Ortiz J V, Izmaylov A F, SonnenbergJ L, Williams-Young D, Ding F, Lipparini F, Egidi F, Goings J, Peng B, Petrone A, Henderson T, Ranasinghe D, Zakrzewski V G, Gao V A, Rega N, Zheng G, Liang W, Hada M, Ehara M, Toyota K, Fukuda R, Hasegawa J, Ishida M, Nakajima T, Honda Y, Kitao O, Nakai H, Vreven T, Throssell K, Montgomery J A, Peralta Jr, J E, Ogliaro F, Bearpark M J, Heyd J J, Brothers E N, Kudin K N, Staroverov V N, Keith T A, Kobayashi R, Normand J, Raghavachari K, Rendell A P, Burant J C, Iyengar S S, Tomasi J, Cossi M, Millam J M, Klene M, Adamo C, Cammi R, Ochterski J W, Martin R L, Morokuma K, Farkas O, Foresman J B & Fox D J, *Gaussian 16, Revision C.01*, (Gaussian, Inc., Wallingford CT) 2016.

33 Parr R G, Yang W, *Density Functional Theory of Atoms and Molecules*, (Oxford University Press, New York) 1989.

34 Dennington R, Keith T A, Millam J M, *GaussView, Version 6*, (Semichem Inc., Shawnee Mission, KS) 2016.

35 McDonald I K & Thornton J M, *J Mol Bio*, 238 (1994) 777.

36 Johnson E R, Keinan S, Mori-Sánchez P, Contreras-García J, Cohen A J, Yang W, *J Am Chem Soc*, 132 (2010) 6498.

37 Lu T & Chen F, *J CompChem,* 33 (2011) 580.

38 Issaoui N, Ghalla H, Muthu S, Flakus H T, Oujia B, *Spe Acta Part A: Mol Biomol Spectro,* 136 (2015) 1227.

39 Lipinski C A, Lombardo F, Dominy B W & Feeney P J, *Adv Drug Del Rev,* 461 (2001) 3.

40 Uma Maheswari J, Muthu S & Tomsundius, *Spectrochim Acta part A,* 137 (2015) 841.

41 Nagabalasubramanian P B, Periandy S, & Mohan S, *Spectro Acta Part A: Molecular and Biomol Spectro,* 77 (2010) 150.

42 Anslyn- Eric V & Dougherty D, *Modern Physical Organic Chemistry,* (University Science) 2006, p. 95.

43 Madhankumar S, Muthuraja P & Dhandapani M, *J Mol Str,* 1181 (2018) 118.

44 Anil kumar J, Dhruvi P, Roshni M, Arpan P & Ketan K, *J Mol Str*, 1181(2019) 295.

45 Okulik N & Jubert A H, *J Mol Des*, 4 (2005) 17.

46 Scrocco E & Tomasi J, *Adv Quantum Chem,* 11 (1978) 115.

47 Luque F J, López J M, & Orozco M, *Theoretical Chem Acc*, 103 (2000) 343.

48 Thul P, Gupta V P, Ram V J & Tandon P, *Spectrochim. Acta A,* 75 (2010) 251.

49 Dennis Raj A, Jeeva M, Shankar M, Purusothaman R, Prabhu G V & Potheher I V, *Phys. B Condens Matter,* 501 (2016) 45.

50 Zeyrek C T, Unver H, Arpacı- O T, Polat K, İskeleli N O & Yildiz M, *J Mol Struct,* 1081 (2015) 22.

51 Govindarajan M, Periandy S & Carthigayen K, *Spectrochim Acta*, A97 (2012) 411.

52 Ravikumar C, Joe I H, Jayakumar V S, *Chem Phys Lett,* 460 (2008) 460.

53 Zaater S, Bouchoucha A, Djebbar S & Brahimi M, *J Mol Struc,* 1123 (2016) 344.

54 Thirumurugan R, Anitha K, *J Mol Struct*, 1146 (9) (2017) 273.

55 Karabacak M, Kurt M, Cinar M, Ayyappan S, Sudha S, Sundaraganesan N, *Spect Acta - Part A Mol Biomol Spect,* 92 (2012) 365.

56 Pearson R G, *Proceed Nat Acad Sci,* 831986 (1986) 8440.

57 Reed A E, Curtiss L A & Weinhold F, *Chem Rev,* 88 (1988) 899.

58 Szafram M, Komasa A, Aamska E B, *J Mol Struct*, 827 (2007) 101.

59 Johnson E R, Keinan S, Mori-Sánchez P, Contreras-García J, Cohen A J & Yang W, *J Am Chem Soc,* 132 (2010) 6498.

60 Contreras-García J, Johnson E R, Keinan S, Chaudret R, Piquemal J P, Beratan D N & Yang W, *J Chem Theory Comp,* 7 (2011) 625.

61 Li Q, Guo X, Yang X, Li W, Cheng, J Li H B, *Phy Chem Chem Phys*, 16 (2014) 11617.

62 Chithiraikumar S, Gandhimathi S & Neelakantan M A, *J Mol Stru*, 1137 (2017) 569.

63 Rizwana B F, Prasana J C, Muthu S, Abraham C S, *Chem Data Coll,* 26 (2020) 100353.

64 Jacobsen H, *Canadian J Chem*, 87 (2009) 695.

65 Silvi B & SavinA, *Nature,* 6499 (1994) 371683.

66 Arulaabaranam K, Mani G & Muthu S, *Chem Data Coll,* 29 (2020) 100525.

67 Govindarajan M, Ali S A, Abdulaziz A, Al-Saadi & Mohamed A I, *Appied Sci,* 5(2015) 955.

68 National Institute of Standards and Technology (NIST). Computational Chemistry Comparison and Benchmark Database: Precomputed Vibrational Scaling Factors. http://cccbdb.nist.gov/vibscalejust.asp.

69 Krishnakumar V & Xavier R J, *Indian J Pure & App Phy,* 41(2003) 597.

70 Srivastava A & Singh V B, *Indian J Pure & App Phy,* 45 (2007) 714.

71 Lin-Vien D, Colthup N B, Fateley W G & Grasselli J G, T*he Handbook of Infrared RamanCharacteristic Frequencies of Organic Molecules*; (Academic Press: Boston, MA, USA) 1991.

72 Arockia doss M, Savithiri S, Rajarajan G, Thanikachalam V & Saleem H, *Spectrochim Acta Part A*, 148 (2015) 189.

73 Silverstein R M, Webster F X & Kiemle D J, *Spectroscopic Identification of Organic Compound*, (John Willey & Sons, New York) 1998 p. 88.

74 Michalska D, Bienko D C, Bienko A J A & Latajka Z, *J Phy Chem,* 100 (1996)17786–17790.

75 Barthes M, De Nunzio G & Ribet M, *Synthetic Metals*, 76 (1996) 337.
76 Panicker C Y, Varghese H T, Philip D, Nogueira H I S & Kastkova K, *Spectrochim Acta,* 67 (2007) 1313.
77 Hasegawa K, Ono T & Noguchi T, *J Phy Chem,* 104 (2004) 4253.
78 Subaschandrabose S, Saleem H, Erdogdu Y, Rajarajan G & Thanikachalam V, *Spectrochim Acta*, 82 (2011) 260.
79 Teimouri A, Chermahini A N, Taban K & Dabbagh H A, *Spectrochim Acta,* 72A (2009) 369.
80 Karthikeyan B, *Spectrochim Acta,* 64A (2006) 1083.
81 Sridevi C, Velraj G, *J Mol Struc,* 1019 (2012) 50.
82 Subramanian N, Sundaraganesan N & Jayabharathi J, *Spectrochim Acta Part A*: *Mol Biomol Spectro,* 76 (2010) 259.
83 Silverstein M, Basseler G C & Morill C, *Spectrometric Identification of Organic Compounds*, (Wiley, New York) 1981.
84 Bunce S J, Edwardsi H G, JohnsonA F, Lewis I R & Turner P H, *Spectrochim Acta,* 49A (1993) 775.
85 Areanas J F, Tocn I L, Orero J C & Marcos J I, *J Mol Structure,* 410 (1997) 443.